

University of Alabama in Huntsville

LOUIS

Theses

UAH Electronic Theses and Dissertations

2012

Static testing of a COTS electric UAV motor in an altitude chamber

Tyler McElroy

Follow this and additional works at: <https://louis.uah.edu/uah-theses>

Recommended Citation

McElroy, Tyler, "Static testing of a COTS electric UAV motor in an altitude chamber" (2012). *Theses*. 595.
<https://louis.uah.edu/uah-theses/595>

This Thesis is brought to you for free and open access by the UAH Electronic Theses and Dissertations at LOUIS. It has been accepted for inclusion in Theses by an authorized administrator of LOUIS.

**STATIC TESTING OF A COTS ELECTRIC UAV MOTOR IN AN ALTITUDE
CHAMBER**

by

TYLER MCELROY

A THESIS

**Submitted in partial fulfillment of the requirements
for the degree of Master of Science in Engineering
in
The Department of Mechanical and Aerospace Engineering
to
The School of Graduate Studies
of
The University of Alabama in Huntsville**

HUNTSVILLE, ALABAMA

2012

In presenting this thesis in partial fulfillment of the requirements for a master's degree from The University of Alabama in Huntsville, I agree that the Library of this University shall make it freely available for inspection. I further agree that permission for extensive copying for scholarly purposes may be granted by my advisor or, in his/her absence, by the Chair of the Department or the Dean of the School of Graduate Studies. It is also understood that due recognition shall be given to me and to The University of Alabama in Huntsville in any scholarly use which may be made of any material in this thesis.

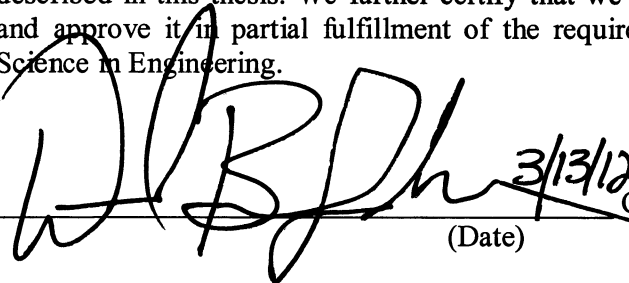

Tyler McElroy

3/15/2012
(Date)


THESIS APPROVAL FORM

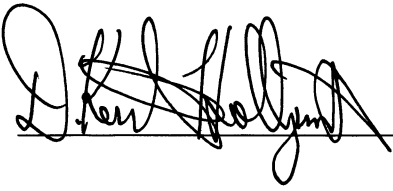
Submitted by Tyler McElroy in partial fulfillment of the requirements for the degree of Master of Science in Engineering and accepted on behalf of the Faculty of the School of Graduate Studies by the thesis committee.

We, the undersigned members of the Graduate Faculty of The University of Alabama in Huntsville, certify that we have advised and/or supervised the candidate on the work described in this thesis. We further certify that we have reviewed the thesis manuscript and approve it in partial fulfillment of the requirements for the degree of Master of Science in Engineering.

 3/13/12
(Date) Committee Chair

 3/13/2012
(Date) Committee Member

 3/14/2012
(Date) Committee Member

 3/14/2012
(Date) Department Chair

 03/14/12
(Date) College Dean

 3/27/12
(Date) Graduate Dean

ABSTRACT

The School of Graduate Studies
The University of Alabama in Huntsville

Degree Master of Science in Engineering College/Dept. Engineering/Mechanical and
Aerospace Engineering

Name of Candidate Tyler McElroy

Title Static Testing of a COTS Electric UAV Motor in an Altitude Chamber

High-altitude unmanned aerial vehicles may benefit from reductions in cost by using commercial off-the-shelf propulsion components. However, little performance data is available for these components. As a step in addressing this issue, a 3-hp electric aircraft motor with a 24 in x 12 in propeller was tested on a static thrust stand within an altitude chamber at pressure altitudes of 0 to 15 km altitudes at constant propeller speeds of 1000 to 5000 RPM. Thrust, input power, propeller RPM, motor temperature, and chamber pressure were measured to characterize motor performance and to verify the experimental set-up. The motor was capable of operating in the low-pressure environment and no mechanical or thermal issues were encountered. Static thrust decreased by approximately 61% between sea-level and 15 km pressure altitudes with a clear trend identified between thrust and air density. Dimensionless thrust, power, and torque coefficients were also estimated. The total uncertainty in the measured and calculated parameters was then assessed with a Monte Carlo simulation.

Abstract Approval: Committee Chair

Department Chair

Graduate Dean





ACKNOWLEDGMENTS

The completion of this thesis was made possible only through the contribution of much time and effort by many individuals, all of whom have earned my deepest gratitude. First, I would like to extend thanks to my advisor and mentor throughout my graduate work, Dr. D. Brian Landrum. He has personally invested countless hours in providing direction for my research, reviewing manuscripts and presentations, offering professional and educational advice, and simply being available to discuss interesting topics in the field of aerospace. My great experience at UAH is largely due to him.

My committee members Dr. Lineberry and Dr. Blackmon have both been directly involved in the preparation of the experimental set-up used for this thesis work. Dr. Blackmon helped in establishing many of the instrumentation and data acquisition methods that were eventually used for this work. Many bugs in the system were identified and fixed thanks to Dr. Lineberry who would always give assistance when requested. Furthermore, both of my committee members have been sources of helpful professional advice.

I also owe gratitude to several of the past and present undergraduates of Dr. Landrum's RoCoRE group. Josiah Thomas was an invaluable asset in fabricating the parts for the test stand and offering excellent suggestions for its design and integration. This thesis would not have even started without his skills. Also, Jonathan McLaury—in addition to suggesting and ordering parts, helping design and build the test stand, and being a good lab assistant—provided guidance on how to operate the motor equipment. Also, thanks to Justin Hanna for giving helpful input on the test stand; it was his ideas that established the essential design.

I would also like to acknowledge Tony Hall of the Propulsion Research Center for instructing me in the operation of the vacuum chamber, offering helpful advice regarding hardware and data acquisition, and simply providing good company.

Several colleagues and friends lent their hands in aiding my thesis work for which I am grateful. Coby McColgin was instrumental in establishing the first iteration of the experimental set-up, including most of the instrumentation and test stand configuration, upon which the new design was derived, as well as writing the DAQ software. Also, Ben Richman helped me on several occasions as an unofficial assistant, choosing to spend his free time in aiding me with testing that lasted well into the evening and on weekends.

Finally, I must acknowledge my ever-supportive family who have consistently and constantly given me not only words but also actions of encouragement throughout my educational career. I wouldn't be where I am today if it wasn't for them.

TABLE OF CONTENTS

	Page
List of Figures	ix
List of Tables.....	xi
List of Symbols	xiii
Chapter	
1. Introduction	1
1.1 Motivation.....	1
1.2 Previous Efforts.....	2
1.3 Scope of Research	3
2. The Experimental Set-Up.....	5
2.1 Background	5
2.2 Propulsion Sub-System Components	7
2.3 Test Stand Design.....	10
2.4 Instrumentation and Data Acquisition	11
3. Test Operation and Analysis	16
3.1 Procedures and Data Reduction	16
3.2 Performance Analysis	17
3.3 Uncertainty Analysis Methodology.....	19
4. Results	22

4.1	Measured and Estimated Propulsive Performance	22
4.2	Nondimensional Performance Parameters	25
4.3	Impact of Uncertainty on Results	27
4.4	Thrust Correlation with Density	29
4.5	Thermal Response	31
5.	Conclusions and Recommendations for Future Work	34
	Appendix A: Load Cell Calibration Data	38
	Appendix B: Measured Performance Data	40
	Appendix C: Calculated Performance Data	43
	Appendix D: Measurement, Elemental, and Propagated Uncertainty Data	46
	References	57

LIST OF FIGURES

Figure	Page
2.1 Experimental set-up for initial series of COTS motor thermal tests at simulated altitudes.	6
2.2 COTS propulsion components (clockwise, starting top-left): motor, transmitter, battery, propeller, ESC.....	9
2.3 Test assembly mounted in the altitude chamber.....	11
2.4 Clockwise, starting top-left: load cell, electronic logger, pressure transducer.	12
2.5 Motor and thrust stand assembly in the altitude chamber.....	13
4.1 Measured thrust vs. propeller RPM.	23
4.2 Measured power supplied to motor vs. propeller RPM.	23
4.3 Calculated induced power vs. propeller RPM.....	24
4.4 Calculated induced torque vs. propeller RPM.....	24
4.5 Thrust coefficient, C_T , vs. propeller RPM.....	25
4.6 Power coefficient, C_P , vs. propeller RPM.....	26
4.7 Torque coefficient, C_Q , vs. propeller RPM.	26
4.8 Ideal static efficiency, η_{st} , vs. propeller RPM.	27
4.9 Average pressure measurements for all tests.	28
4.10 Thrust coefficient, C_T , vs. density ratio, δ , with associated power function and exponential function best-fit curves.	29
4.11 Maximum temperature achieved while motor was operating.	32
4.12 Maximum temperature achieved after motor shut down.	32

A.1 Generated calibration curves for load cell with C50-15XL motor and 24 x 12 in propeller mounted on thrust stand.	38
D.1 Convergence of Monte Carlo simulation results for total normalized uncertainty (U_X/X) of thrust for all 0 km tests.	50
D.2 Convergence of Monte Carlo simulation results for total normalized uncertainty (U_X/X) of pressure for all 15 km tests.	50

LIST OF TABLES

Table	Page
2.1 COTS propulsion components.	9
2.2 List of instrumentation and manufacturer-specified systematic uncertainties.	14
A.1 Thrust load cell calibration data.	39
B.1 Test matrix; test #10 at 5 km, 5000 RPM set point not completed.	40
B.2 Measured propulsive and chamber condition data and calculated density for 0 km altitude.	40
B.3 Measured propulsive and chamber condition data and calculated density for 5, 10, and 15 km altitudes.	41
B.4 Measured thermal response data for all altitudes.	42
C.1 Calculated propulsive data for 0 and 5 km altitudes.	43
C.2 Calculated propulsive data for 10 and 15 km altitudes.	44
C.3 Calculated dimensionless coefficients for 0 and 5 km altitudes.	44
C.4 Calculated dimensionless coefficients for 10 and 15 km altitudes.	45
D.1 Random uncertainty bands ($\pm U/2$) for all measured parameters for 0 and 5 km altitudes.	46
D.2 Random uncertainty bands ($\pm U/2$) for all measured parameters for 10 and 15 km altitudes.	47
D.3 Elemental systematic uncertainty sources and associated bands ($\pm U/2$) for thrust measurements for all altitudes.	48
D.4 Elemental systematic uncertainty sources and associated bands ($\pm U/2$) for electrical and temperature measurements for all altitudes.	49

D.5 Total uncertainty bands ($\pm U/2$) for all measured parameters for all altitudes.....	51
D.6 Total uncertainty bands ($\pm U/2$) for all calculated performance parameters for all altitudes.	52
D.7 Total uncertainty bands ($\pm U/2$) for all calculated dimensionless coefficients for all altitudes.	53
D.8 Total uncertainty percentages (U_X/X) for all measured parameters for all altitudes...	54
D.9 Total uncertainty percentages (U_X/X) for all calculated performance parameters for all altitudes.	55
D.10 Total uncertainty percentages (U_X/X) for all calculated dimensionless coefficients for all altitudes.....	56

LIST OF SYMBOLS

English Symbol	Definition
C_P	coefficient of power
C_Q	coefficient of torque
C_T	coefficient of thrust
D	propeller diameter, ft
e_{rms}	normalized root-mean-square deviation
I	current, A
N	number of samples
n	propeller rotation rate, RPM
P	power, hp
p	pressure, atm
Q	torque, lb-ft
R	specific gas constant, lb-ft/slug-°R
s	random uncertainty
T	thrust, lb
U	total uncertainty
V	voltage, V
X	measurement

Greek Symbol	Definition
β	systematic uncertainty

δ	density ratio
ε	error
η_{st}	ideal static efficiency
θ	temperature, °F
μ	mean
ρ	air density, slug/ft ³
σ	standard deviation

Subscripts	Definition
0	sea-level conditions
i	induced
j, k	variable indexes
m	measured
sp	supplied
tr	trend

CHAPTER 1

INTRODUCTION

1.1 Motivation

Over the last decade, unmanned aerial vehicles (UAVs) have seen a significant increase in the numbers of individual craft being deployed as well as the numbers of available configurations, mission profiles, operators, and customers of UAV-based services. Though UAVs have historically been used primarily in military applications, the civil and commercial sectors have started to take interest in using unmanned aircraft. Furthermore, UAVs have gradually begun to carry out what were traditionally manned roles in addition to uniquely unmanned applications.

As the UAV market and its associated technology continues to mature, designers and operators have naturally sought to reduce costs in the production and maintenance of UAVs as well as achieving shorter development times for new vehicle designs. One method of achieving this end is the use of commercial off-the-shelf (COTS) components, particularly in an aircraft's propulsion sub-system [1]. COTS motors (both internal combustion and electric), propellers, batteries, and other related hardware are generally designed exclusively for R/C model aircraft enthusiasts. Manufacturers typically only provide "hobbyist-level" part specifications that are limited to operational and safety

information rather than detailed performance data. Even when data is available, it often comes in the form of online databases composed of test data collected from R/C aircraft enthusiasts whose experimental methods are typically not published (much less, documented) and have not been vetted by any overseeing party or entity. Additionally, most of this performance information is only applicable to the narrow flight regimes that interest model aircraft enthusiasts (relatively low altitudes and very short flight times). This can pose a problem for designers interested in implementing COTS components in UAVs, especially for non-conventional vehicle configurations and high-altitude, long-endurance mission profiles. It is also difficult to apply traditional conceptual design and performance prediction methods without appropriate performance data [2].

1.2 Previous Efforts

A handful of studies have been carried out in recent years to address this knowledge gap by characterizing the performance of COTS propulsion components. These studies have included both purely computational analyses and physical tests. After performing numerous trade studies of electric motors, propellers, batteries, and control servos, researchers at NASA's Langley Research Center had repeatedly identified the need to conduct extensive testing of COTS components for use in small UAVs [3, 4]. Ol, Zeune, and Logan [5] performed wind tunnel tests at Langley and the Air Force Research Laboratory using several COTS electric motors and propellers, with the focus on characterizing performance of propellers ranging in diameter from 6 in to 20 in. The experimental study was supplemented with numerical analyses of the propellers. Corrigan and Altman [2] at the University of Dayton carried out wind tunnel testing to

determine thrust, power output, and propulsive efficiency of three electric UAV motors (ranging in power from 0.25 hp to 0.80 hp) with various propellers (ranging in diameter from 10 in to 14 in). Dynamometer tests of COTS internal combustion engines ranging in power of 0.25 hp to 9.3 hp were the focus of master's theses by Menon [6] and Moulton [7] of the University of Maryland.

All performance tests conducted thus far—static and wind tunnel-based alike—have been run at sea-level conditions. Review of the relevant literature indicates no testing efforts have yet been made to assess any COTS motor's performance at relatively high altitudes. One of the primary motivators of COTS component performance research is more confident design methodology and performance predictions for new vehicles across many types of flight regimes, including high altitudes. Therefore, altitude testing of these components is a necessary progression to previous work.

1.3 Scope of Research

The work presented in this thesis is a first step in establishing a sustainable testing methodology for COTS propulsion components in high-altitude settings. Constraints imposed by the available facilities, pre-existing resources, and purchasing budget limited the number of components to be tested and the instrumentation to be used. Therefore, a test series was conducted with a single large, high-performance COTS electric motor and propeller mounted to a custom-built test stand capable of measuring thrust. The stand was housed within a large vacuum chamber to simulate the pressure conditions seen at altitude. This test series had two broad objectives: first, to provide partial characterization of the static propulsive performance of the motor at several pressure altitudes ranging up

to 15 km; and second, to assess the usefulness of the experimental set-up (the thrust stand and vacuum chamber combination) in terms of controllability of the test conditions and uncertainty of the measurements and reduced data.

It is envisioned that testing of this nature—conducted either in-house or at other institutions and facilities—can be eventually matured to the point of providing a large base of useful, published performance data for a variety of electric motors and propellers across a wide range of operating conditions. This data could then be used by designers to more confidently employ COTS propulsion components in many types of high-altitude UAV concepts including fixed-wing, rotary-wing, and airship designs across a multitude of mission profiles in both the civil, commercial, and military aircraft sectors.

CHAPTER 2

THE EXPERIMENTAL SET-UP

2.1 Background

A previous test series was performed to investigate the thermal performance of a statically-mounted motor and its related components at pressure altitudes of 0, 10, and 20 km within a large vacuum chamber [8]. The effects of passive thermal management with cooling fins were also studied. This effort did not include any measurements of the motor's propulsive performance (thrust, power, etc.) aside from propeller RPM. The motor was found to be capable of operating at a pressure altitude of up to 20 km, but was prone to overheating at the higher altitudes.

This initial experimental series was important in three basic ways. First, it demonstrated the feasibility of using a vacuum chamber as a means of testing an electric motor in a simulated high-altitude environment. Second, it established much of the instrumentation set-up and the data-acquisition methods used in carrying out the experimental work for this thesis. Third, it provided a very useful base of experience for operation of the COTS propulsion components and the chamber itself, as well as data collection, reduction, and analysis methods. This initial experimental set-up within the vacuum chamber is shown in Figure 2.1.

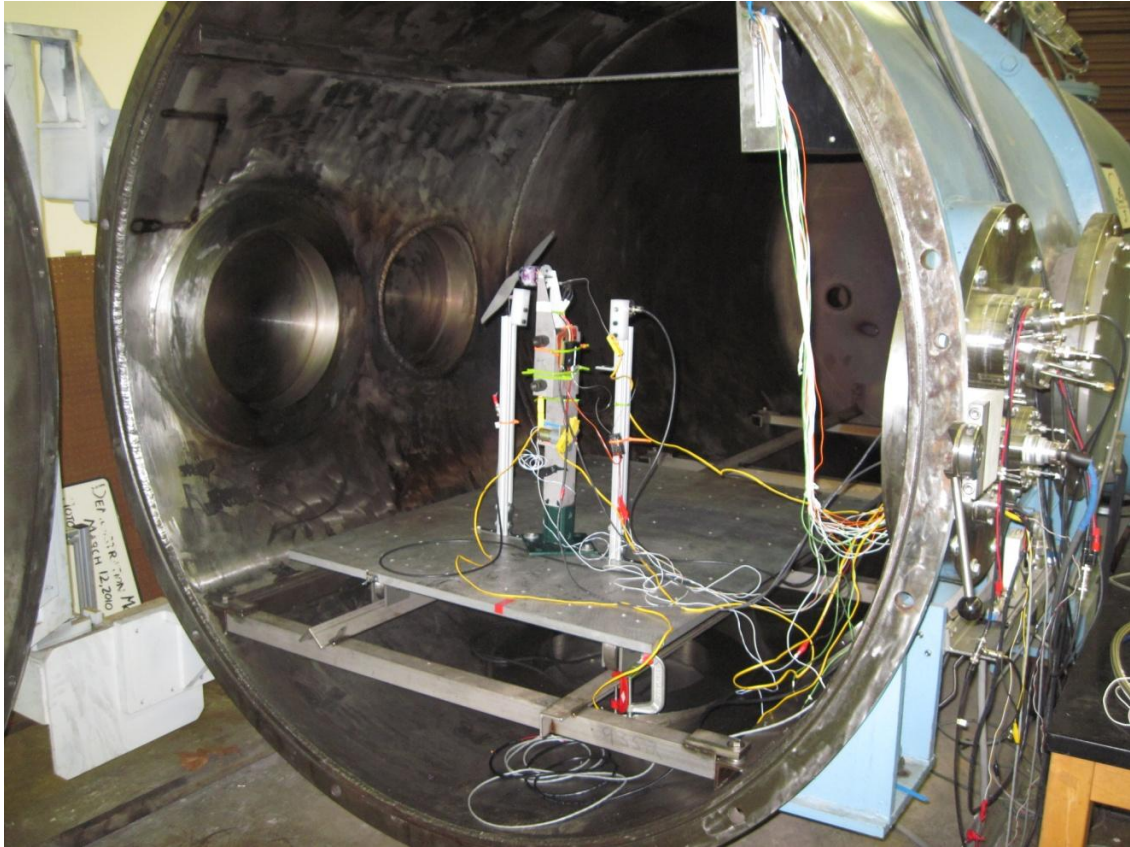


Figure 2.1 Experimental set-up for initial series of COTS motor thermal tests at simulated altitudes.

The design of the stand seen in Figure 2.1 precluded the possibility of safely or economically implementing any sort of method of thrust or torque measurement. To characterize a motor's propulsive performance, fabrication of a new test stand was required. However, elements of the original test stand were able to be adapted into the newer design, helping to reduce costs and fabrication time.

The vacuum chamber is housed in the Propulsion Research Center (PRC) at the University of Alabama in Huntsville (UAH). The large chamber measures 6 ft in diameter and 13 ft in length and is capable of achieving high vacuum (10^{-10} atm). Only a rough vacuum environment was needed to simulate the atmospheric pressures expected

for high-altitude UAVs. An important aspect of the chamber's design is that it is only capable of controlling pressure. The internal chamber temperature is affected by the ambient conditions of the facility it is housed within. Therefore, only pressure altitude, rather than density altitude, was simulated for all tests. The use of the chamber also precluded the possibility of simulating forward flight as would be possible in a wind tunnel. As such, static conditions were assumed for determining performance. The confined internal chamber volume would result in low levels of air re-circulation induced by the propeller. However, these effects were considered to be negligible given the very large volume of the chamber and are not considered in the experimental results.

2.2 Propulsion Sub-System Components

A single motor and propeller were used during the test series for this thesis. The selection of the motor was driven partly on experience with the motor of the initial test series. This previous motor was a brushless "outrunner" type in which the motor case spins along with the drive shaft. This configuration has the advantage of producing greater torque at lower speeds and consequently does not require a gearbox. Difficulties in monitoring motor case temperature arose with the outrunner configuration. Therefore, when the next series of tests was planned, it was decided that a traditional "inrunner" motor with a gearbox would be used.

The Hacker C50-15XL brushless motor equipped with a 6.7:1 planetary gearbox was selected and fixed with an APC 24 in x 12 in electric propeller. The manufacturer recommends a 22 in x 12 in propeller for use with the C50-15XL [9]. However, because

the motor would be operated at simulated altitudes where the air density is significantly lower than in nominal conditions, a slightly larger propeller was deemed appropriate.

Electrical power was supplied to the motor via a 37-V, 10-cell lithium-polymer (Li-Po) battery pack. A regulated DC power supply would be the ideal choice for operating the motor. However, the selected motor is rated at a maximum power of about 3 hp (2200 W at 37 V and 60 A). Therefore, to provide a useful assessment of the motor across its full operating range, any power supply would be required to operate at least near those power levels. Unfortunately, the PRC does not have access to a regulated power supply this large, and time and budget restrictions prohibited the acquisition of such a unit. As a result, the rechargeable Li-Po battery packs had to be used. Consequently, the length of each individual test was limited by the batteries' capacity and the current draw of the motor.

Given that Li-Po chemistry cells have a tendency to explode if not handled correctly, the risk of battery rupture inside the chamber at reduced pressures was considered too great. Therefore, the packs were placed outside of the chamber with power fed to the internally mounted motor. Initially, two packs were available in order to reduce turn-around time between individual tests. However, one of the packs was found to be defective and was only briefly used before being deemed unsafe. Only a single pack was used for all main tests.

Motor speed was controlled externally with a radio transmitter. The earlier test series had shown that an external radio signal was capable of penetrating into the chamber interior. A receiver within the chamber powered by an independent, external battery pack relayed the throttle inputs to the electronic speed controller (ESC) which in

turn operated the motor. The propulsion-related components are summarized in Table 2.1 and are shown in Figure 2.2.

Table 2.1 COTS propulsion components.

Component	Description/Details
Motor	Hacker C50-15XL Acro Competition w/ 6.7:1 Gearbox
ESC	Hacker MasterSPIN 99 Opto
Propeller	APC 24 in x 12 in, Electric
Battery Pack	Thunder Power TP5000-10SPL2 5000 mAh 10S Li-Po
Transmitter/Receiver	Futaba LXXGG2 8-Channel 2.4 GHz

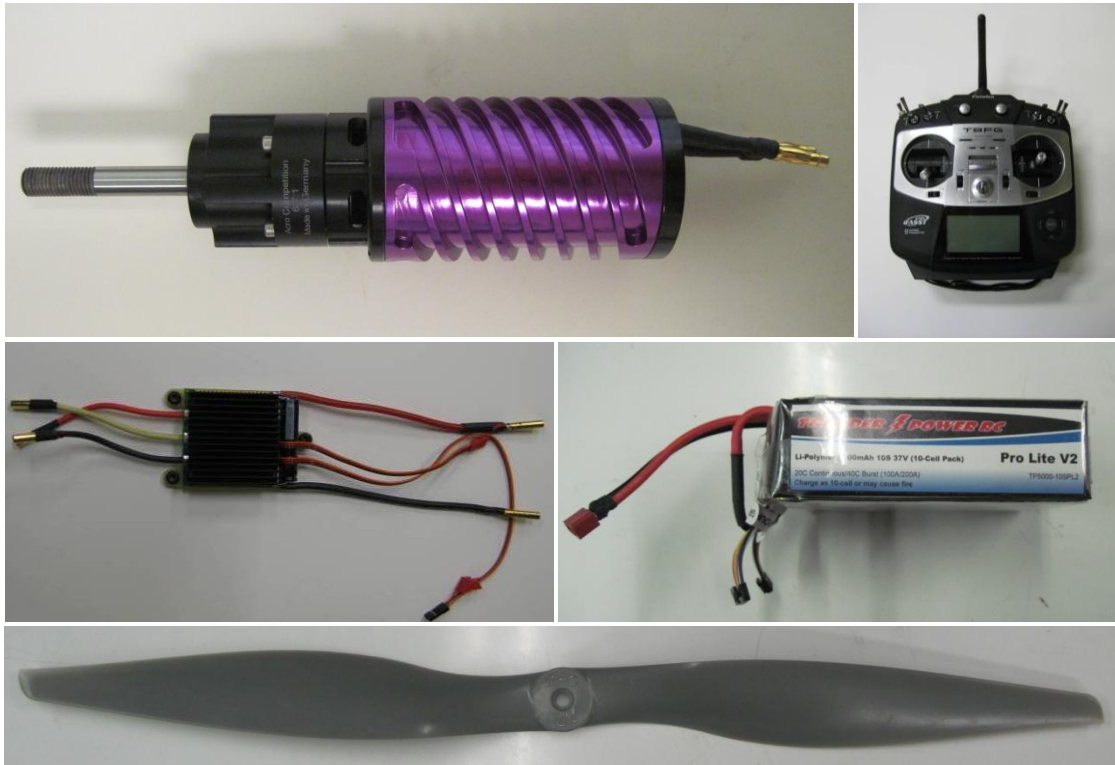


Figure 2.2 COTS propulsion components (clockwise, starting top-left): motor, transmitter, battery, propeller, ESC.

2.3 Test Stand Design

A static thrust stand was designed and fabricated specifically for use within the altitude chamber. The thrust stand needed to be as simple and economical as possible while still providing measurements within a reasonable uncertainty level. The PRC chamber's design placed several constraints on installing any structure within it. The chamber interior has a single mounting plate capable of being moved longitudinally along the chamber's length. A vertical motor orientation was ruled out due to concerns regarding adequate structural torsional rigidity as well as ignoring the advantage afforded by aligning the motor along the chamber's longest axis so as to minimize air recirculation. Conversely, any horizontally orientated configuration required adequate clearance between the mounting plate and propeller disk edge.

The resulting thrust stand is shown in Figure 2.3. The design consists of a lever arm pinned at one end so it is free to rotate independently. The motor is mounted at the other end of the arm. A column is fixed to the chamber plate and is linked to the lever arm by a coupling to keep the entire assembly in static equilibrium. A 25-lb capacity load cell makes up a portion of this coupling in order to measure the thrust developed by the propeller. Budget and time restrictions prevented the implementation of any sort of method of output torque measurement. As such, total output power could not be determined and direct propulsive measurement was limited to only static thrust.

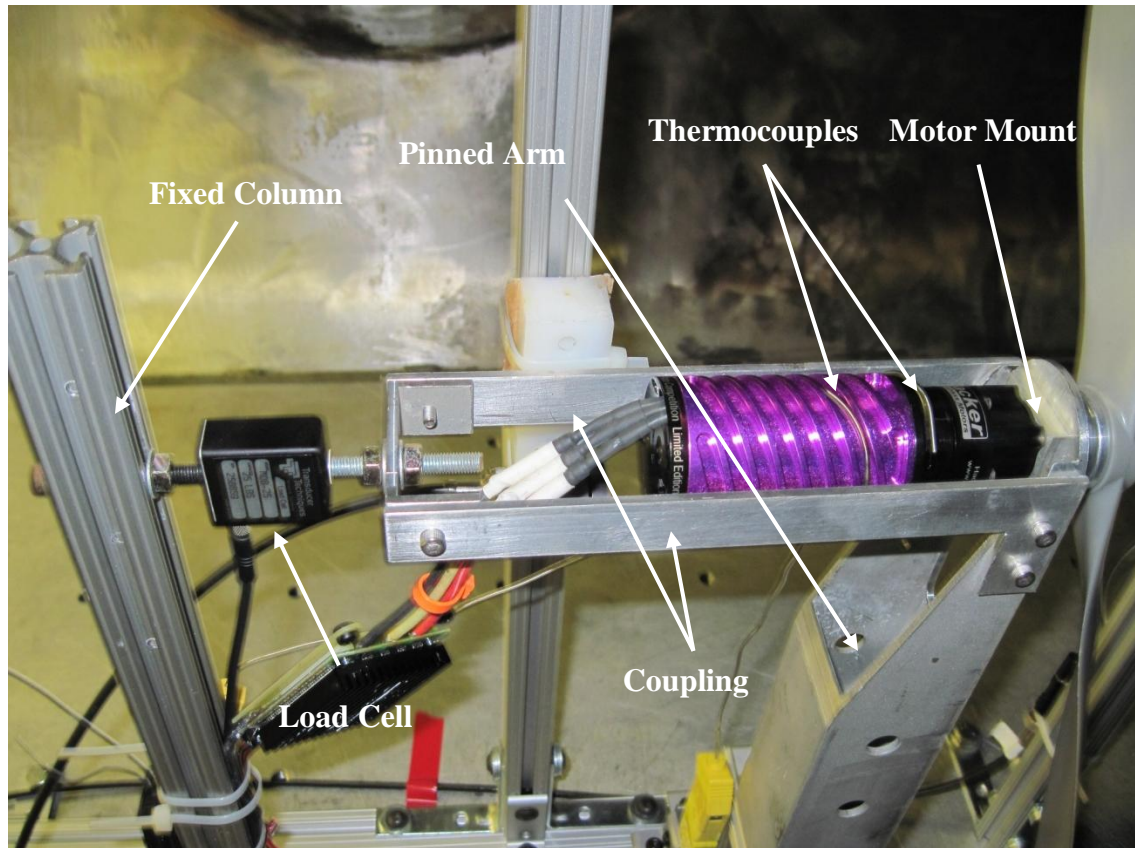


Figure 2.3 Test assembly mounted in the altitude chamber.

2.4 Instrumentation and Data Acquisition

The load cell was calibrated while integrated with the entire thrust stand and motor assembly to eliminate installation errors. Force was applied to the motor along its axis of rotation by connecting a line from the propeller hub to a hook suspended from a mounted pulley. Various weights were hung while output voltage was recorded to produce a calibration curve. The voltage response of the load cell was measured for both increasing and decreasing loads in order to assess any hysteresis error. The resulting calibration data and trend lines are provided in Appendix A.

A COTS data logging module was used to measure the voltage supplied by the battery pack (V_{sp}) and the current drawn by the motor (I_{sp}) so that the power supplied (P_{sp}) to the motor could be calculated by

$$P_{sp} = V_{sp} I_{sp} \cdot \quad (2.1)$$

Chamber pressure was monitored with a wall-mounted P-type thermocouple rough vacuum gauge. The load cell, data logger, and vacuum gauge are all show in Figure 2.4.

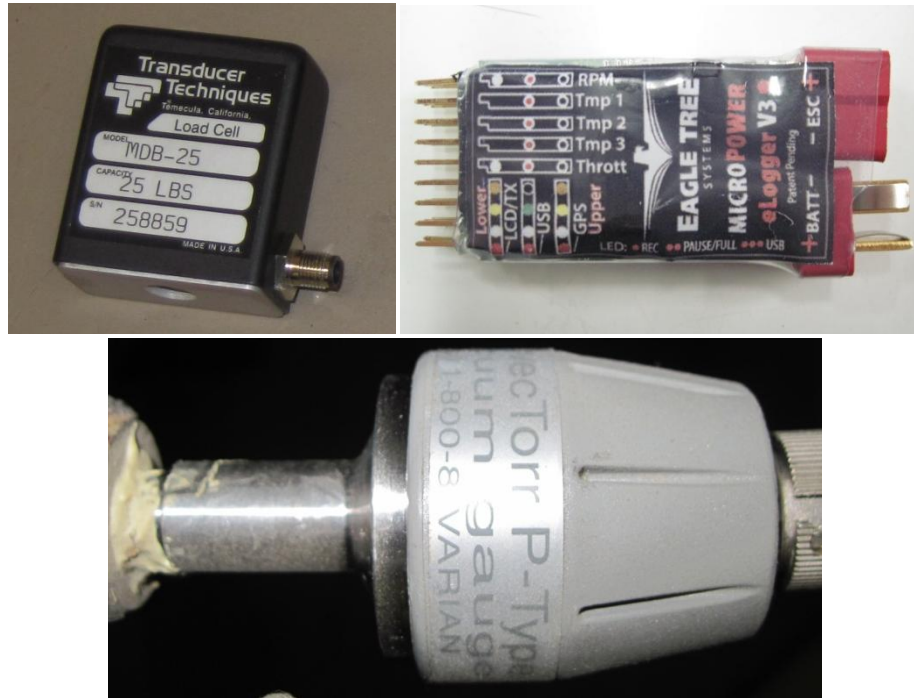


Figure 2.4 Clockwise, starting top-left: load cell, electronic logger, pressure transducer.

Propeller RPM was measured by an optical tachometer assembly that had been developed for the earlier thermal test series. It consisted of a bright, white LED-based light source on the far side of the propeller disk. Coaxial to the light on the opposing side

of the propeller disk was a high-speed photodetector. The output signal from the photodetector is processed through a software-based bandpass filter to attenuate any low- or high-frequency harmonics excited by vibrations induced by the motor or buffeting from the propwash. The propeller's rotation rate is then determined by counting the number of pulses of the detector's filtered signal within a given period. The instrumented thrust stand assembly as housed within the altitude chamber and selected sensors are shown in Figure 2.5.

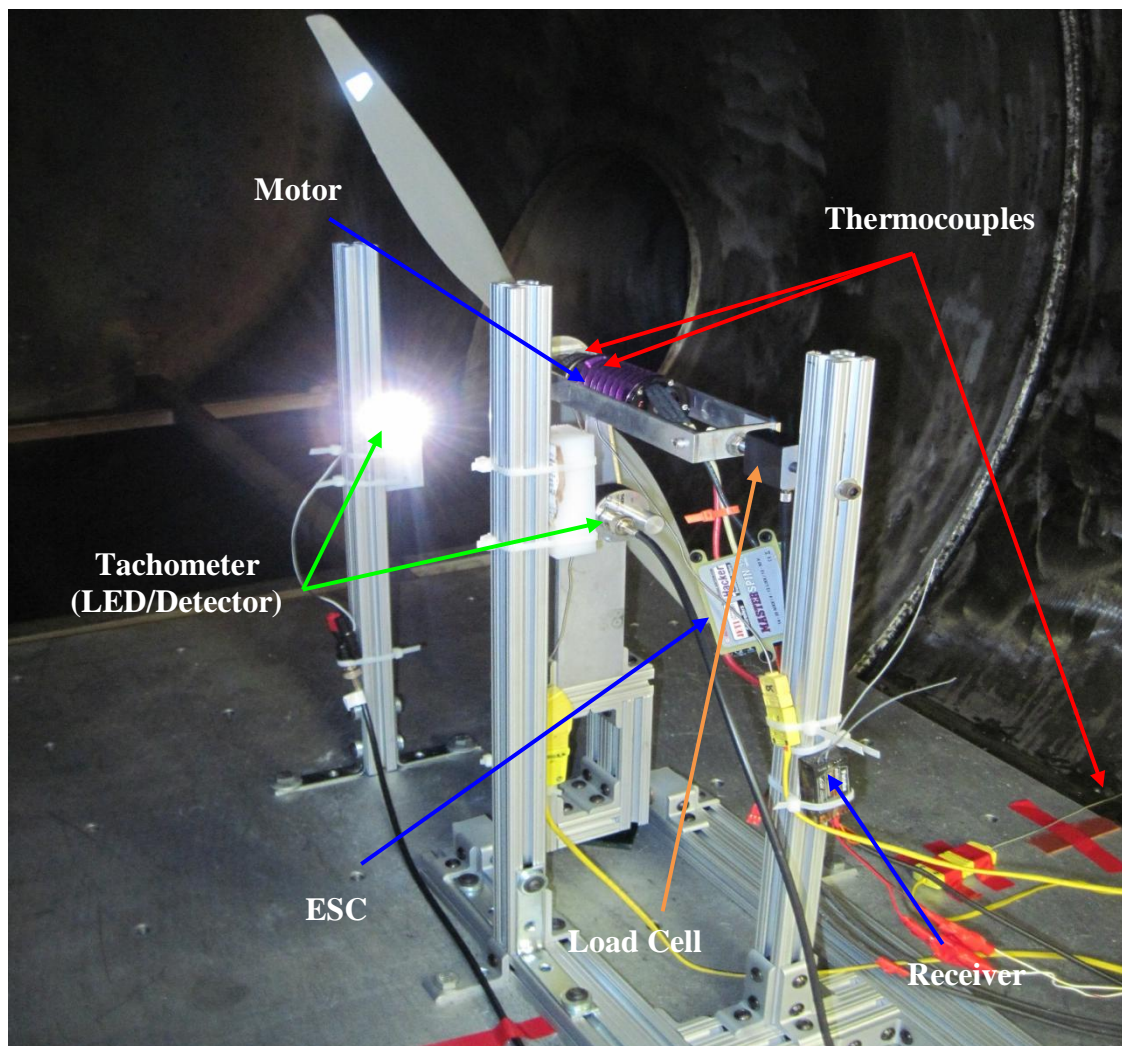


Figure 2.5 Motor and thrust stand assembly in the altitude chamber.

The surface temperature of the gearbox and motor case were monitored with separate thermocouples wrapped around each component (specific placement can be seen in Figure 2.3). The temperature of the altitude chamber's interior was sensed by another thermocouple probe placed where the surrounding air would be minimally affected by the propwash and any heat flux emitted from the motor (seen at the far right of Figure 2.5). Table 2.2 lists the test instrumentation and available manufacturer-rated uncertainties. These uncertainties were derived from References 10, 11, and 12.

Table 2.2 List of instrumentation and manufacturer-specified systematic uncertainties.

Sensor/Measurement	Description/Details	Systematic Uncertainty
Load Cell/Thrust	Transducer Techniques MDB-25	± 0.011 lb
Wattmeter/Supplied Voltage and Current	Eagle Tree Systems eLogger V3	± 0.02 V, ± 0.01 A
Tachometer/Propeller Speed	Optical Pulse Counter: White LED Light Source/ThorLabs DET210 Photodetector	N/A (Considered negligible relative to random uncertainty)
Thermocouples/Temperature	Omega Type-K Thermocouples with CJC	$\pm 2.3^{\circ}\text{F}$
Vacuum Gauge/Pressure	Varian ConvecTorr P-Type Rough Vacuum Gauge	N/A (Considered negligible relative to random uncertainty)

Data acquisition consisted of essentially two separate systems routed to a single controlling terminal. For the first and primary DAQ set-up, most of the instrumentation output was connected to a laptop computer via a portable USB-based analog-to-digital converter. The resulting signals were then monitored, manipulated, and recorded using LabVIEW[®]. Though each sensor had different sampling frequencies, only one sample per

second was recorded for each measurement in the output data file. The second set-up only acquired the output from the COTS data logger which was also connected via USB to the computer. Data was interpreted, displayed, and recorded at 10 samples per second using software designed exclusively for the logger module. Since two separate systems were used for recording all measurements, the data of the two resulting files had to be synchronized in time. This was accomplished by simply noting the rapid rise in thrust from the LabVIEW[®] file and current draw from the COTS logger file. The time values for each file were then initialized to the one corresponding to the motor start transient.

CHAPTER 3

TEST OPERATION AND ANALYSIS

3.1 Procedures and Data Reduction

A total of 20 individual tests were planned for this series. These included constant propeller speeds of 1000, 2000, 3000, 4000, and 5000 RPM at each pressure altitude of 0, 5, 10, and 15 km. Each test was performed only once. All tests were started with a freshly recharged battery pack and run until either the motor temperature had achieved steady-state or the battery pack had been discharged to the point that constant speed operation was no longer possible. The motor temperature was monitored after shutdown to observe the temperature spike that resulted from loss of convective cooling from the propwash. Additionally, a new test was not conducted until the motor temperature had returned to within at least 5°F of the chamber's interior temperature. The thermal data is given in Appendix B.

The length of each test ran between 300 and 600 seconds in order to allow the motor to achieve steady-state temperature or as near to that condition as battery life would permit. However, for the propulsive performance parameters, a data set that large was not required. A set of representative data points was selected from a 20-second time span during which the measurements were qualitatively determined to be at steady-state.

The 20-second sample was always drawn from the first 100 seconds of recorded data. From this sample, the mean was calculated for each individual span of measurement data. The resulting averages were then used as the nominal values for each reduced data point. These data points are presented in Appendix B.

A more detailed study of the data verified that the values of the mean and standard deviation for each parameter varied negligibly between different 20-second selections as long as the sample was drawn from the first 100 seconds of data and after the motor start transient. As such, the qualitative method of data selection described earlier was used for all tests.

3.2 Performance Analysis

Although the experimental set-up was incapable of providing a direct measurement of motor torque and output power, a rough estimation of these parameters could still be determined using classic momentum theory [13]. The ideal induced power P_i applied to the air for a static propeller is calculated by

$$P_i = \frac{T^{3/2}}{\sqrt{\pi \rho D^2 / 2}} . \quad (3.1)$$

The resulting induced torque Q_i is then derived using propeller RPM by

$$Q_i = \frac{P_i}{2\pi n} . \quad (3.2)$$

It is important to note that the values determined by Equations (3.1) and (3.2) are unattainable in reality due to losses from profile drag, tip trailing vortices, and any stalled regions of the propeller blades.

Since the power supplied to the motor (P_{sp}) is known, an ideal static propulsive efficiency η_{st} can then be defined by

$$\eta_{st} = \frac{P_i}{P_{sp}}. \quad (3.3)$$

This efficiency parameter includes both the effects of mechanical losses in the motor's power train and the static propulsive efficiency of the propeller. Again, since the true value of the usable power applied to the flow will always be smaller than P_i , η_{st} is the absolute upper limit on the total efficiency of the motor/propeller. The parameter defined in Equation (3.3) is specifically called a "static propulsive efficiency" to differentiate it from true propulsive efficiency which, by definition, is zero for the static case. For rotorcraft, this parameter is called the figure of merit [13] and is used to gauge rotor performance during hover. However, since the motor is being used to drive a propeller intended for forward-flight operation, the η_{st} symbol will be exclusively used from here on to distinguish these results from those for rotorcraft.

Performance data are typically published in a nondimensional form where the performance of the motor is normalized against the size and operating conditions of the propeller. For the purposes of this thesis, the respective nondimensional thrust, torque, and power coefficients are defined as

$$C_T = \frac{T}{\rho n^2 D^4}, \quad (3.4)$$

$$C_Q = \frac{Q_i}{\rho n^2 D^5}, \text{ and} \quad (3.5)$$

$$C_P = \frac{P_{sp}}{\rho n^3 D^5}, \quad (3.6)$$

where the air density, ρ , is calculated with the ideal gas law

$$\rho = \frac{P}{R\theta}. \quad (3.7)$$

Because these coefficients are normally reported as functions of advanced ratio—which itself is a function of forward flight speed— C_T , C_Q , and C_P are usually not very useful in the static case [14]. However, by representing the nondimensional coefficients as functions of propeller RPM, the motor's performance can still be assessed in a mechanical sense rather than in the traditional propulsive manner used for forward flight operation. The calculated dimensional and nondimensional performance parameters are tabulated in Appendix C.

3.3 Uncertainty Analysis Methodology

The second objective of this study was to validate the test stand design by way of an uncertainty analysis of both the measured and calculated data. This was achieved by conducting an Excel[®] spreadsheet-based Monte Carlo simulation for all test runs, using a methodology suggested by Coleman and Steele [15].

The results of the uncertainty analysis are presented in Appendix D. For each measured parameter—thrust, propeller RPM, supplied voltage and current, temperature, and chamber pressure—a set of Gaussian error distributions was assumed for each individual random and/or systematic uncertainty source. Each error distribution was defined by a standard deviation (σ) and a mean (μ). The random error source distributions were defined by the standard deviation (σ_s) of each measured parameter (calculated from each 20-second set of data points during the main data reduction) and centered about a mean of zero. The systematic sources, when applicable, were generally based on manufacturer specifications for each sensor (load cell, wattmeter, and thermocouples) as given in Table 2.2. All specified systematic uncertainty values (U_{sys}) were assumed to be at a 95-percent confidence level. As such, the standard deviation (β) required for each systematic error distribution was assumed to be half of the uncertainty value where

$$\beta = 0.5U_{sys}. \quad (3.8)$$

Only a single systematic error distribution was used (if at all) for the parameters during the simulation. The standard deviation (σ_β) used for defining each systematic error distribution was determined by the square root of the sum of the squares of each systematic uncertainty source:

$$\sigma_\beta = \left[\sum_j (\beta_j)^2 \right]^{1/2}. \quad (3.9)$$

These systematic error distributions were also centered about a mean of zero.

The mean value of each parameter was assumed to be the nominal or “true” measurement (X_{true}). A random number generator then selected an error value (ε) from each error source distribution. The resulting errors from the random and systematic distributions were then summed with the nominal value to simulate a single measurement (X) subjected to some error:

$$X = X_{true} + \sum_k^N (\varepsilon_{s,k} + \varepsilon_{\beta,k}) . \quad (3.10)$$

At this point, any calculated parameters (such as the dimensionless coefficients) were computed from the simulated error-containing measured values (X). The simulation was then run for 1000 iterations. Convergence of the results was observed to generally occur between about 200 and 600 iterations, examples of which can be seen in Figures D.1 and D.2 of Appendix D. This resulted in each parameter having a 1000-point distribution affected by both direct and propagated sources of error. The standard deviation (σ_X) was calculated for each 1000-point distribution, indicating the value of uncertainty of all the parameters. This uncertainty was then expanded to a 95-percent confidence level by multiplying σ_X by 2, resulting in the total uncertainty (U) of every parameter.

CHAPTER 4

RESULTS

4.1 Measured and Estimated Propulsive Performance

Figures 4.1 and 4.2 present the measured thrust and the power supplied to the motor, respectively. The maximum recorded static thrust was 21.4 lb for a power consumption of 3.1 hp at the 0 km pressure altitude and 5000 RPM. Minimum thrust was 0.31 lb with a power consumption of 0.01 hp at the 15 km pressure altitude and 1000 RPM. In general, measured thrust decreased for increasing pressure altitudes at a fixed propeller RPM as would be expected due to lower air densities. Similarly, power consumed by the motor decreased as pressure altitude increased and loading on the motor dropped.

The induced power and induced torque values were calculated using Equations (3.1) and (3.2), respectively. Figures 4.3 and 4.4 show that these parameters, when plotted with respect to propeller RPM, display trends similar to those for thrust and supplied power. However, the induced power and torque do not decrease simply with altitude. The 0 km values are greatest (as would be expected), but it is clear that the 15 km values are actually larger than the 5 and 10 km points.

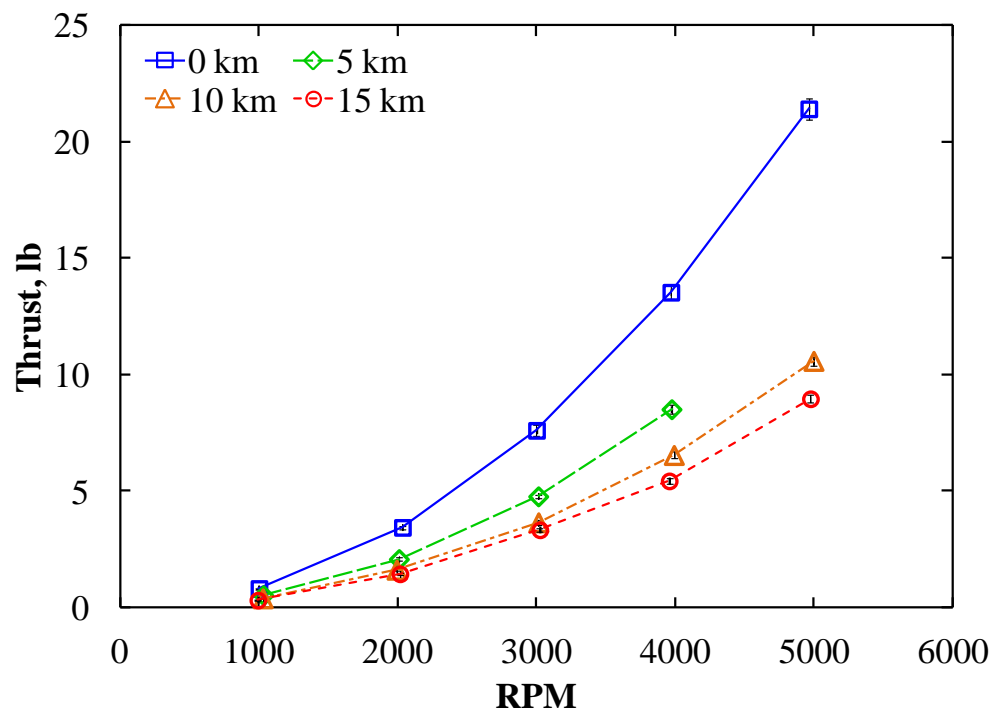


Figure 4.1 Measured thrust vs. propeller RPM.

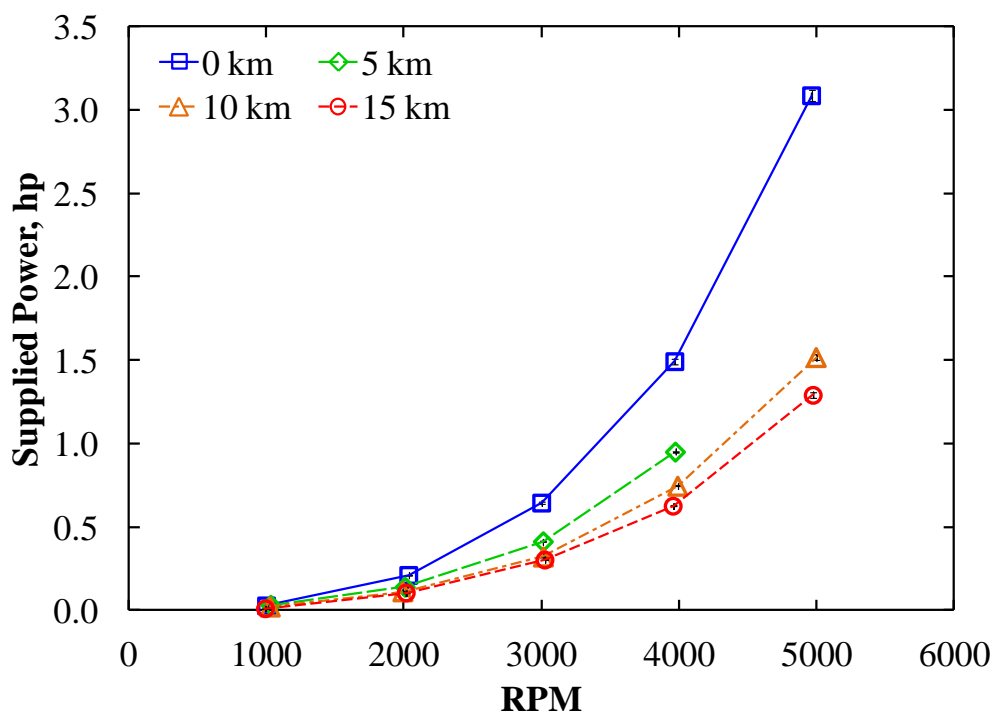


Figure 4.2 Measured power supplied to motor vs. propeller RPM.

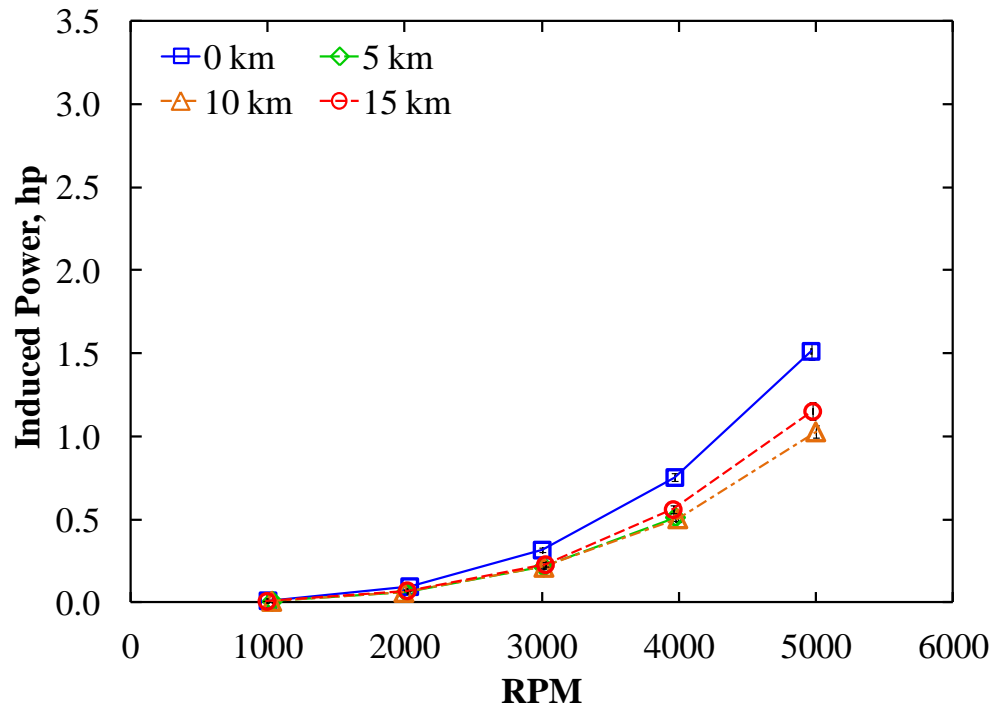


Figure 4.3 Calculated induced power vs. propeller RPM.

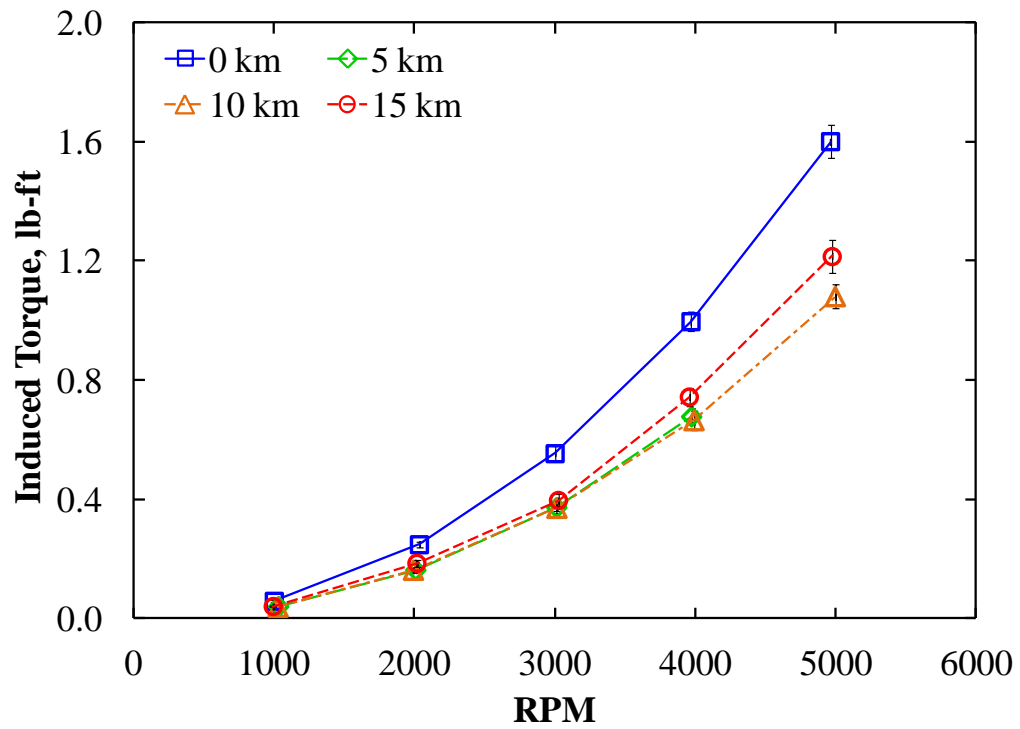


Figure 4.4 Calculated induced torque vs. propeller RPM.

4.2 Nondimensional Performance Parameters

The nondimensional coefficients of C_T , C_P , and C_Q and the ideal static efficiency η_{st} are presented in Figures 4.5 to 4.8, respectively. Apart from the 15 km data, the thrust coefficients (Figure 4.5) and torque coefficients (Figure 4.7) increase only slightly for increasing propeller RPM at a given pressure altitude. In Figure 4.6, the power coefficients decrease with propeller RPM for pressure altitudes of 5 and 10 km whereas the 0 km C_P appears to have a local minimum between 3000 and 4000 RPM. The 15 km data does not present an easily interpreted trend. Figure 4.8 shows the static efficiencies at the lower three altitudes following the inverse of the trends seen in the power coefficient plot. The ideal static efficiency has a local maximum around 4000 RPM for the 0, 5, and 10 km altitudes. The 15 km data do not follow a clear trend.

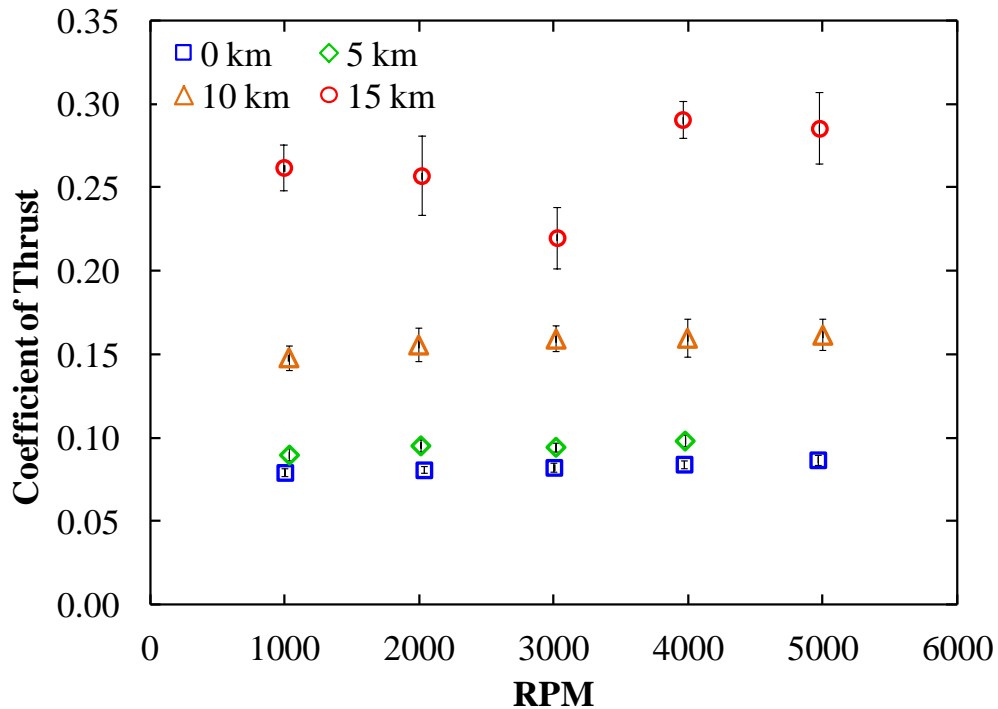


Figure 4.5 Thrust coefficient, C_T , vs. propeller RPM.

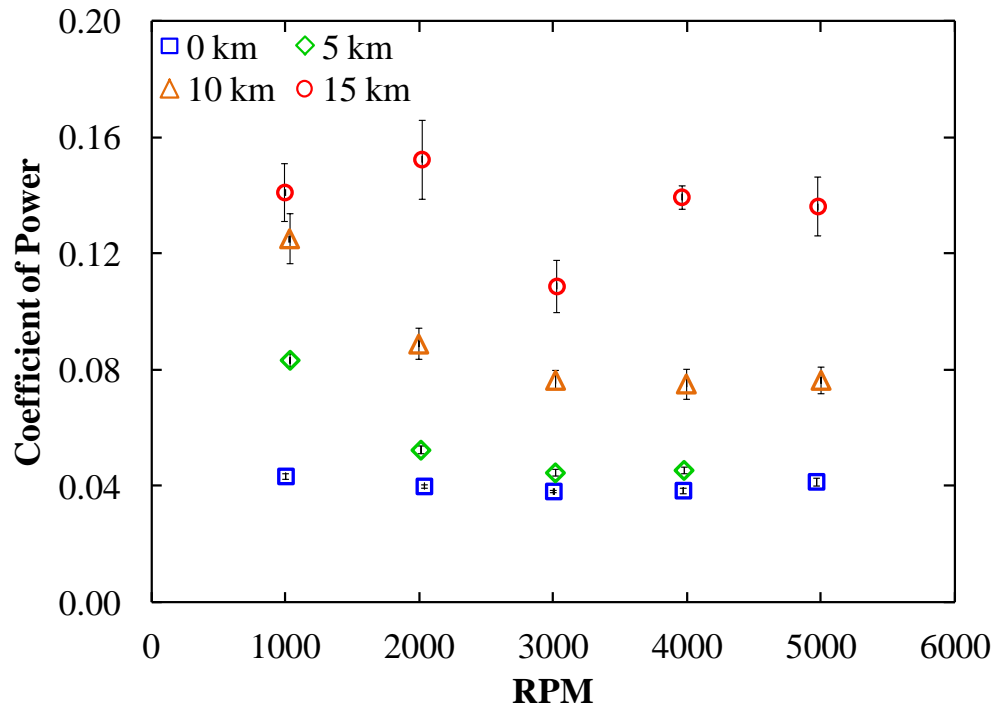


Figure 4.6 Power coefficient, C_P , vs. propeller RPM.

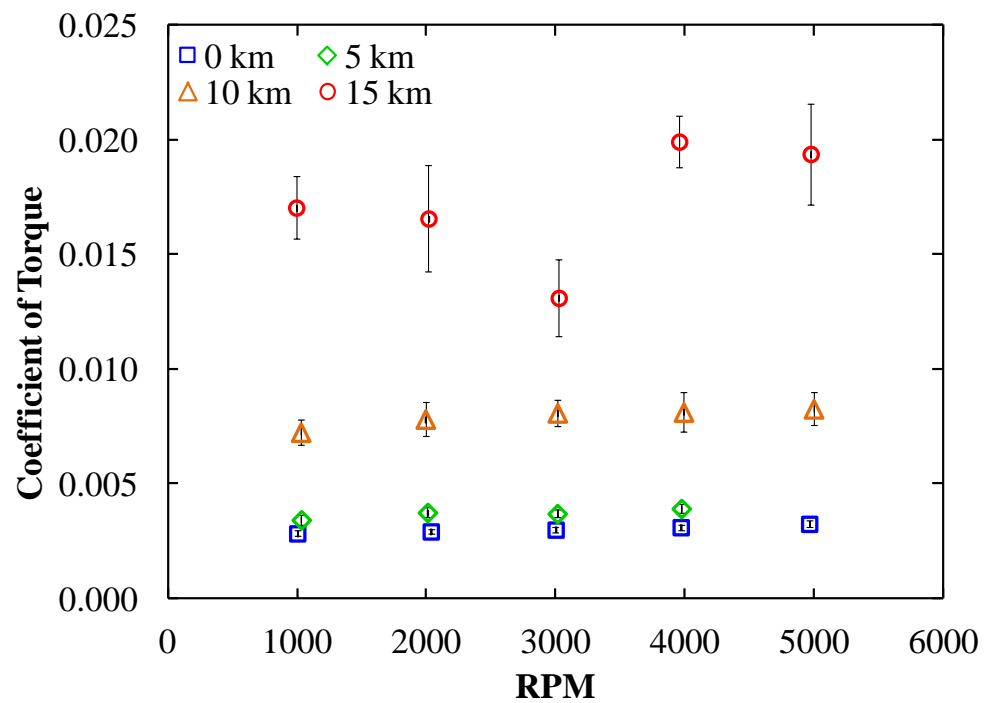


Figure 4.7 Torque coefficient, C_Q , vs. propeller RPM.

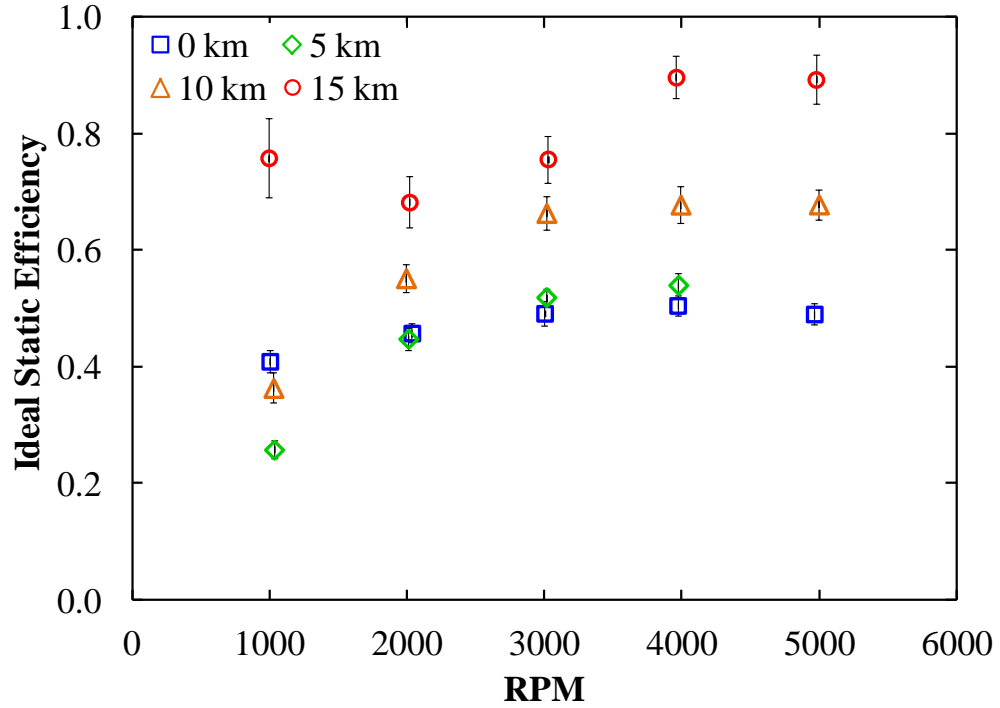


Figure 4.8 Ideal static efficiency, η_{st} , vs. propeller RPM.

4.3 Impact of Uncertainty on Results

Generally, for all of the plots of Figures 4.5 to 4.8, the scatter and resultant uncertainty values of the data points increase with pressure altitude. This is most obvious in the 15 km data sets with several uncertainties for the torque coefficient between 20 and 30 percent of the nominal value. While conducting the uncertainty analysis, it was observed that the pressure measurement contributed between 70 and 80 percent of the total uncertainty of the dimensionless coefficients. Figure 4.9 presents the nominal pressure readings and their associated uncertainties across the five propeller speeds and four intended altitudes.

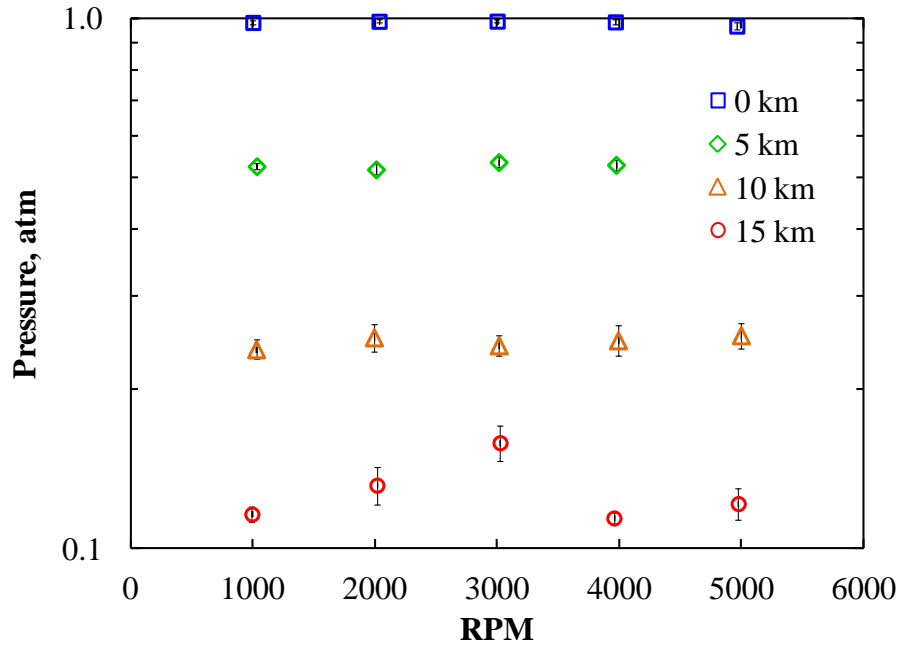


Figure 4.9 Average pressure measurements for all tests.

The uncertainties of the individual pressure measurements increased with pressure altitude from less than 3 percent at 0 km to over 15 percent at 15 km. Even as testing was conducted, the pressure reading was observed in real time to vary significantly at the higher pressure altitudes. The fluctuations in the pressure measurements also made it difficult to maintain a consistent pressure level between tests at the 15 km altitude. Due to the low air density in the chamber at this highest altitude, cooling of the motor back to ambient levels could take well in excess of an hour. This provided sufficient time for air to leak back into the chamber, lowering the pressure altitude by several kilometers, and thereby requiring a short chamber pumpdown. However, difficulty in reading the pressure accurately (to within 0.01-0.02 atm) resulted in inconsistent pressures across the five tests at 15 km and, to a lesser extent, at 10 km. It can be readily seen that for the 15-km series, the pressure steadily increased for the first three tests after which the chamber

was pumped down to the initial level. The pressure then increased again for the last test. Close examination of the error bars also indicates a general increase in uncertainty levels at the higher pressure altitudes.

4.4 Thrust Correlation with Density

As seen in Figure 4.1, the thrust clearly decreases with increasing altitude for any given RPM setting. This observation extends also to the dimensionless thrust coefficients shown in Figure 4.5. This trend is expected with higher altitudes because the air density will consequently decrease, and the propeller will have less fluid upon which to do work. In order to explicitly identify this trend, the thrust coefficient is plotted against a dimensionless density ratio, δ , in Figure 4.10

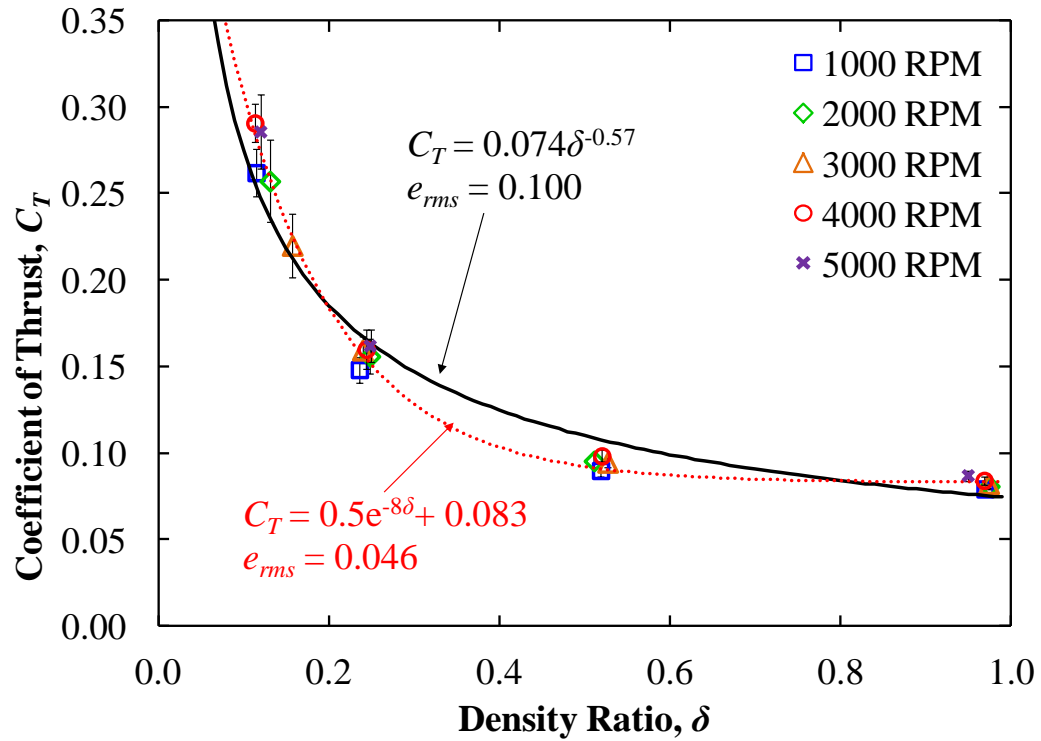


Figure 4.10 Thrust coefficient, C_T , vs. density ratio, δ , with associated power function and exponential function best-fit curves.

The density ratio is a normalization of the calculated air density within the chamber and is given by

$$\delta = \frac{\rho}{\rho_0}, \quad (4.1)$$

where ρ_0 is standard sea-level air density which was defined as 0.00237 slug/ft³. As seen Figure 4.10, by presenting the thrust coefficients as a function of density, the results of all tests are essentially “collapsed” into a single trend regardless of RPM setting.

Two curve fits are shown in Figure 4.10 as an attempt to quantify the relationship of thrust and density for the motor and propeller that were used. One curve is expressed by the power function

$$C_T = 0.074\delta^{-0.57}, \quad (4.2)$$

while the other curve is expressed by the exponential function

$$C_T = 0.5e^{-8\delta} + 0.083. \quad (4.3)$$

The equations for both curves are accompanied by their respective normalized root-mean-square deviations, e_{rms} , as a means to quantify their goodness of fit to the data. The normalized deviation is determined by

$$e_{rms} = \sqrt{\frac{1}{N} \sum_j \left[\frac{(X_{m,j} - X_{tr,j})^2}{X_{m,j}^2} \right]}. \quad (4.3)$$

Based on the normalized deviations for both curves, the exponential function of Equation (4.3), with an average deviation of about 5 percent, provides a better fit to the data points than Equation (4.2), with an e_{rms} of about 10 percent. However, expressing the trend of Figure 4.10 as a power function allows the relationship of thrust and density to be reduced down to a constant, seen by simply rearranging Equation (4.2) to obtain

$$C_T \delta^{0.57} = 0.074 . \quad (4.4)$$

The value of 0.074 is essentially a dimensionless number that describes the static thrust performance of the C50-15XL motor with a 24 in x 12 in propeller across all densities and propeller RPMs. Though Equations (4.2) and (4.4) do not express this thrust/density relationship quite as precisely as Equation (4.3), it still allows for a reasonable estimation of static thrust at any density, especially considering the uncertainty levels of the thrust coefficients that are already present.

4.5 Thermal Response

The thermal responses of the motor and gearbox were measured both while the motor was actively running and for about 300 seconds after it was shut down. Tabularized temperature data are shown in Appendix B. Figure 4.11 presents the maximum temperature achieved while the motor was active, and Figure 4.12 shows the maximum temperature attained after shutdown. In both cases, the temperatures are plotted against power consumed by the motor.

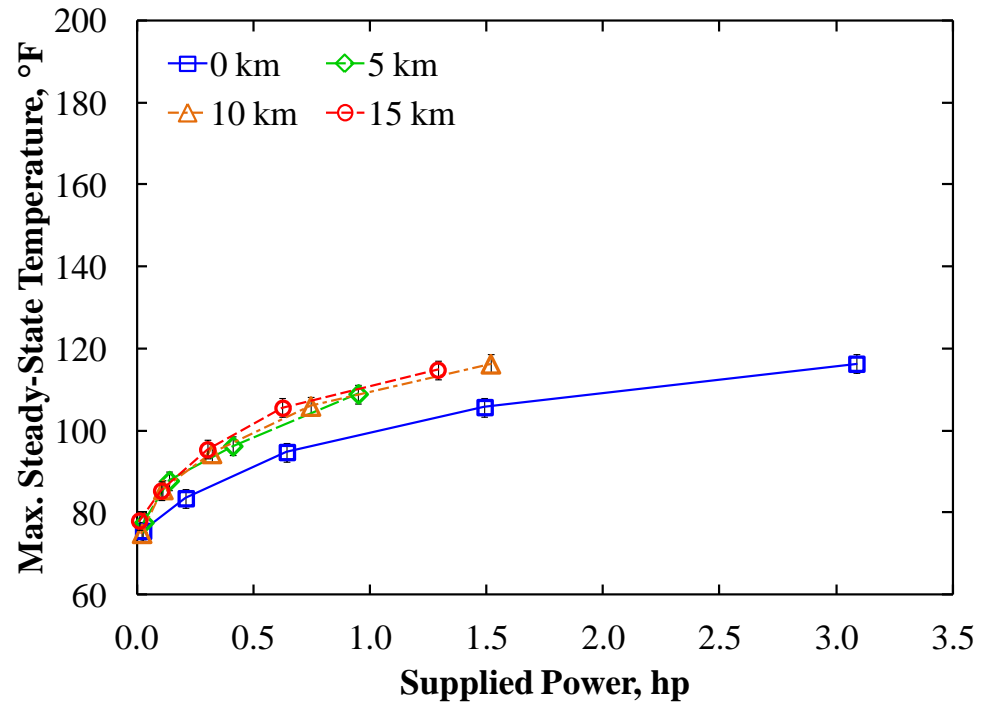


Figure 4.11 Maximum temperature achieved while motor was operating.

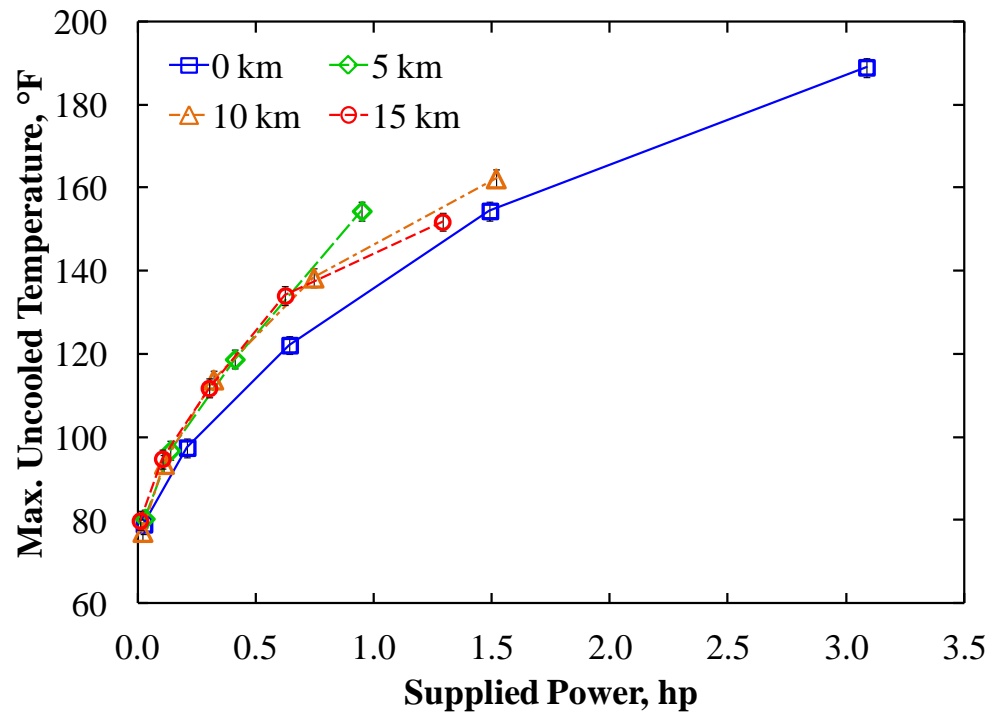


Figure 4.12 Maximum temperature achieved after motor shut down.

Concern had been raised during test planning that the gearbox might be more susceptible to overheating than the motor itself due to the mechanical stress imposed on it by reducing the output speed. However, in all tests the gearbox's temperature was within 1-3°F of the motor case. The motor used in the previous thermal test series was shown to be susceptible to overheating at higher pressure altitudes, presumably due to decreasing air density and consequently less convective cooling via propwash. In contrast, the motor for this study was capable of remaining adequately cool up to the maximum rated power of 3 hp across all four altitudes as long the propeller remained in motion. By referencing Figures 2.2 and 2.3 again, it can be seen that the motor has a helical, fin-like cut along its case, improving heat rejection to the surrounding air. However, if the convective cooling supplied by the propwash is cut off, then temperature can spike significantly higher, exceeding the assumed maximum operating temperature of 180°F, and overheating the motor. This is only a concern for static operation. In forward flight, the oncoming freestream airflow should cool the motor in the event of a power-out scenario.

CHAPTER 5

CONCLUSIONS AND RECOMMENDATIONS FOR FUTURE WORK

The selected motor was capable of operating in the low-pressure environment within the vacuum chamber. Static thrust, input power, propeller speed, and motor case temperature were measured with reasonable uncertainty levels ranging from about 2 percent up to a maximum of 12 percent. The calculated performance parameters of induced power, induced torque, and ideal static efficiency also had generally acceptable levels of uncertainty near 10 percent—especially at pressure altitudes of 0, 5, and 10 km. Uncertainty levels for the dimensionless coefficients are, for the most part, also reasonable at the lowest pressure altitudes of 0, 5, and 10 km.

Nondimensional performance of the motor at the highest pressure altitude of 15 km is more difficult to ascertain with uncertainty levels ranging from 15 to 30 percent. Specifically, the values of C_Q have the highest uncertainties among all the calculations. However, because C_P was defined by the supplied power, and C_Q was calculated from a simple estimate of induced torque, these performance parameters should only be considered as rough indicators of output power and torque. As such, the levels of uncertainty in these parameters are not of great concern.

Efforts can be made to further reduce the sources of uncertainty currently present in the experimental set-up. Additional bracing added to the thrust stand could significantly reduce the effect of induced mechanical vibrations on the thrust and propeller speed measurements, making them more precise. The variability seen in the vacuum gauge is a problem that needs to be addressed if testing is to progress using this altitude chamber at pressure altitudes greater than 10 km. It is unclear whether the fluctuations are inherent for this gauge at lower pressures or, perhaps, they are due—in whole or in part—to the re-circulating airflow induced within the chamber. Examination of the error bands for the pressure measurements across the 19 individual tests do not appear to show any clear trend between increased propeller speed and increased uncertainty. However, the fluctuations might only arise for certain propeller speeds due to some unique coupling between the chamber geometry and the level of air re-circulation. The simplest solution to reducing uncertainty in the pressure reading would be to circumvent the vacuum gauge altogether and install a different static pressure transducer within the chamber.

If the problems identified above can be adequately solved, a second test series should be conducted to assess the repeatability of the results. Following this verification, additional static testing of this motor could continue with several other propellers of various diameters and pitches. The smaller outrunner motor of the initial test series can also be installed on the thrust stand to gauge its static propulsive performance for several different propellers. Additionally, it would be very useful to modify the existing thrust stand at some point to incorporate a method of torque measurement so that output power could be determined.

A basic correlation was derived between the thrust coefficient and density ratio. This relationship can be used for rapid estimation of the performance of similar motor/propeller combinations across various altitudes. This correlation method could then be applied to the measured torque and power coefficients to observe whether any useful trends also occur for these parameters with density. The resulting correlations could also be extended to other motor/propeller combinations.

No thermal issues were observed during operation of the motor at any altitude. However, only the pressure environment of the altitude chamber was controllable, and the effects of actual in-flight temperature conditions (which are significantly colder at the altitudes at which this testing was performed) on this type of motor are not known. Therefore, low-temperature effects on COTS electric motor performance need to be studied. Additionally, supplementing this static, high-altitude data with results from low-speed wind tunnel testing would also be a good way of more fully assessing a motor's performance during actual forward flight.

APPENDICES

APPENDIX A

LOAD CELL CALIBRATION DATA

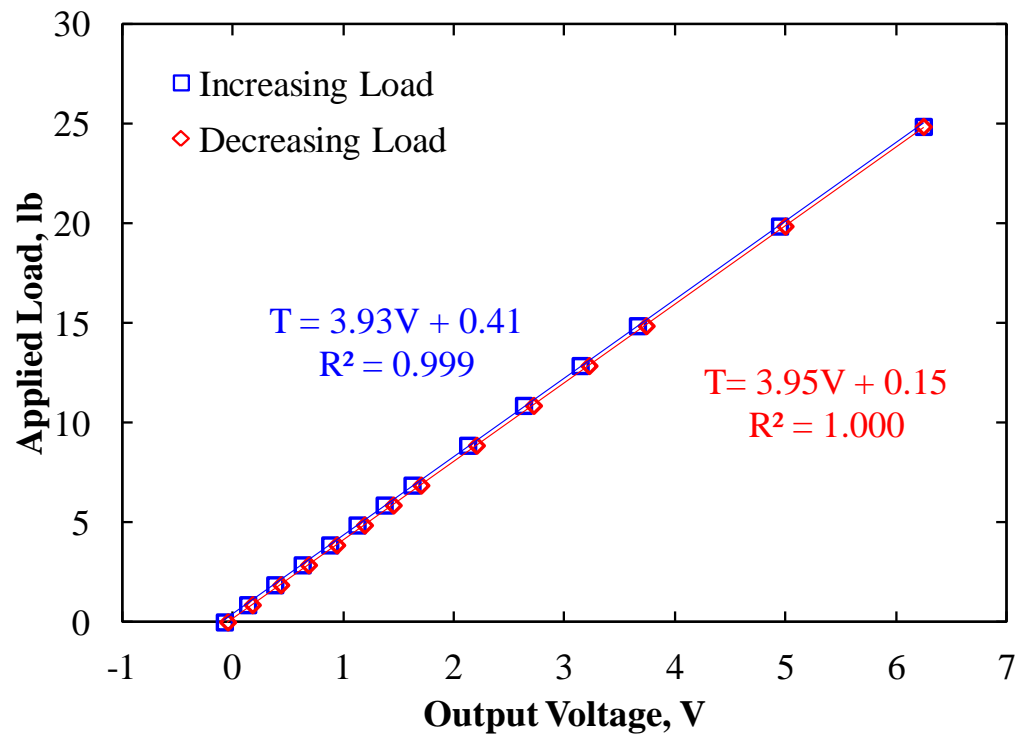


Figure A.1 Generated calibration curves for load cell with C50-15XL motor and 24 x 12 in propeller mounted on thrust stand.

Table A.1 Thrust load cell calibration data.

	Output Voltage (V)	Applied Load (lb)
Increasing Load	-0.075	0.000
	0.136	0.865
	0.381	1.865
	0.629	2.865
	0.878	3.865
	1.125	4.865
	1.370	5.865
	1.622	6.865
	2.125	8.865
	2.630	10.865
	3.142	12.865
	3.660	14.865
	4.945	19.865
Max. Load	6.245	24.865
Decreasing Load	4.995	19.865
	3.739	14.865
	3.222	12.865
	2.720	10.865
	2.204	8.865
	1.702	6.865
	1.452	5.865
	1.192	4.865
	0.941	3.865
	0.686	2.865
	0.435	1.865
	0.178	0.865
	-0.045	0.000

APPENDIX B

MEASURED PERFORMANCE DATA

Table B.1 Test matrix; test #10 at 5 km, 5000 RPM set point not completed.

Test No.		Propeller RPM				
		1000	2000	3000	4000	5000
Pressure Altitude	0 km	1	2	3	4	5
	5 km	6	7	8	9	10 (NC)
	10 km	11	12	13	14	15
	15 km	16	17	18	19	20

Table B.2 Measured propulsive and chamber condition data and calculated density for 0 km altitude.

Altitude: 0 km					
RPM	Pressure (atm)	Density (slug/ft ³)	Thrust (lb)	Supplied Power (hp)	Ambient Temp. (°F)
1001	0.98	0.00230	0.81	0.03	68
2035	0.99	0.00231	3.43	0.21	68
3002	0.99	0.00231	7.60	0.64	69
3970	0.99	0.00230	13.5	1.49	70
4964	0.97	0.00225	21.4	3.09	71

Table B.3 Measured propulsive and chamber condition data and calculated density for 5, 10, and 15 km altitudes.

Altitude: 5 km					
RPM	Pressure (atm)	Density (slug/ft ³)	Thrust (lb)	Supplied Power (hp)	Ambient Temp. (°F)
1032	0.53	0.00123	0.52	0.03	69
2009	0.52	0.00121	2.07	0.14	69
3014	0.54	0.00125	4.77	0.41	70
3974	0.53	0.00123	8.51	0.95	71
—	—	—	—	—	—
Altitude: 10 km					
RPM	Pressure (atm)	Density (slug/ft ³)	Thrust (lb)	Supplied Power (hp)	Ambient Temp. (°F)
1028	0.24	0.00056	0.39	0.02	65
1993	0.25	0.00059	1.62	0.11	65
3015	0.24	0.00057	3.65	0.32	66
3991	0.25	0.00058	6.54	0.74	68
4998	0.25	0.00059	10.6	1.52	69
Altitude: 15 km					
RPM	Pressure (atm)	Density (slug/ft ³)	Thrust (lb)	Supplied Power (hp)	Ambient Temp. (°F)
993	0.12	0.00027	0.31	0.01	67
2017	0.13	0.00031	1.44	0.10	64
3025	0.16	0.00037	3.33	0.30	65
3958	0.11	0.00027	5.43	0.63	65
4976	0.12	0.00029	8.96	1.29	66

Table B.4 Measured thermal response data for all altitudes

Altitude: 0 km			
RPM	Pressure (atm)	Max. S-S Temp. (°F)	Max. Uncooled Temp. (°F)
1001	0.98	75	79
2035	0.99	83	97
3002	0.99	95	122
3970	0.99	106	154
4964	0.97	116	189
Altitude: 5 km			
RPM	Pressure (atm)	Max. S-S Temp. (°F)	Max. Uncooled Temp. (°F)
1032	0.53	78	80
2009	0.52	88	97
3014	0.54	96	119
3974	0.53	109	154
—	—	—	—
Altitude: 10 km			
RPM	Pressure (atm)	Max. S-S Temp. (°F)	Max. Uncooled Temp. (°F)
1028	0.24	75	77
1993	0.25	86	93
3015	0.24	94	114
3991	0.25	106	138
4998	0.25	116	162
Altitude: 15 km			
RPM	Pressure (atm)	Max. S-S Temp. (°F)	Max. Uncooled Temp. (°F)
993	0.12	78	80
2017	0.13	85	95
3025	0.16	95	112
3958	0.11	106	134
4976	0.12	115	152

APPENDIX C

CALCULATED PERFORMANCE DATA

Table C.1 Calculated propulsive data for 0 and 5 km altitudes.

Altitude: 0 km				
RPM	Pressure (atm)	Induced Power (hp)	Induced Torque (ft-lb)	Ideal Efficiency
1001	0.98	0.01	0.06	41%
2035	0.99	0.10	0.25	46%
3002	0.99	0.32	0.55	49%
3970	0.99	0.75	1.00	50%
4964	0.97	1.51	1.60	49%
Altitude: 5 km				
RPM	Pressure (atm)	Induced Power (hp)	Induced Torque (ft-lb)	Ideal Efficiency
1032	0.53	0.01	0.04	26%
2009	0.52	0.06	0.16	45%
3014	0.54	0.21	0.37	52%
3974	0.53	0.51	0.68	54%
—	—	—	—	—

Table C.2 Calculated propulsive data for 10 and 15 km altitudes.

Altitude: 10 km				
RPM	Pressure (atm)	Induced Power (hp)	Induced Torque (ft-lb)	Ideal Efficiency
1028	0.24	0.01	0.04	36%
1993	0.25	0.06	0.16	55%
3015	0.24	0.21	0.37	66%
3991	0.25	0.50	0.66	68%
4998	0.25	1.03	1.08	68%
Altitude: 15 km				
RPM	Pressure (atm)	Induced Power (hp)	Induced Torque (ft-lb)	Ideal Efficiency
993	0.12	0.01	0.04	76%
2017	0.13	0.07	0.19	68%
3025	0.16	0.23	0.40	76%
3958	0.11	0.56	0.74	90%
4976	0.12	1.15	1.22	89%

Table C.3 Calculated dimensionless coefficients for 0 and 5 km altitudes.

Altitude: 0 km				
RPM	Pressure (atm)	Thrust Coeff.	Power Coeff.	Torque Coeff.
1001	0.98	0.079	0.043	0.0028
2035	0.99	0.081	0.040	0.0029
3002	0.99	0.082	0.038	0.0030
3970	0.99	0.084	0.039	0.0031
4964	0.97	0.087	0.042	0.0032
Altitude: 5 km				
RPM	Pressure (atm)	Thrust Coeff.	Power Coeff.	Torque Coeff.
1032	0.53	0.090	0.083	0.0034
2009	0.52	0.095	0.052	0.0037
3014	0.54	0.095	0.045	0.0037
3974	0.53	0.098	0.046	0.0039
—	—	—	—	—

Table C.4 Calculated dimensionless coefficients for 10 and 15 km altitudes.

Altitude: 10 km				
RPM	Pressure (atm)	Thrust Coeff.	Power Coeff.	Torque Coeff.
1028	0.24	0.15	0.13	0.0072
1993	0.25	0.16	0.089	0.0078
3015	0.24	0.16	0.077	0.0081
3991	0.25	0.16	0.075	0.0081
4998	0.25	0.16	0.077	0.0083
Altitude: 15 km				
RPM	Pressure (atm)	Thrust Coeff.	Power Coeff.	Torque Coeff.
993	0.12	0.26	0.14	0.017
2017	0.13	0.26	0.15	0.017
3025	0.16	0.22	0.11	0.013
3958	0.11	0.29	0.14	0.020
4976	0.12	0.29	0.14	0.019

APPENDIX D

MEASUREMENT, ELEMENTAL, AND PROPAGATED UNCERTAINTY DATA

Table D.1 Random uncertainty bands ($\pm U/2$) for all measured parameters for 0 and 5 km altitudes.

Altitude: 0 km						
Nominal RPM	Measured RPM	Pressure (atm)	Thrust (lb)	Supplied Voltage (V)	Supplied Current (A)	Ambient Temp. (°F)
1000	4	0.007	0.02	0.00	0.00	0.0
2000	5	0.007	0.07	0.02	0.03	0.0
3000	8	0.007	0.22	0.07	0.07	0.1
4000	22	0.009	0.28	0.09	0.32	0.0
5000	44	0.016	0.46	0.16	0.63	0.2
Altitude: 5 km						
Nominal RPM	Measured RPM	Pressure (atm)	Thrust (lb)	Supplied Voltage (V)	Supplied Current (A)	Ambient Temp. (°F)
1000	5	0.007	0.01	0.01	0.03	0.0
2000	6	0.011	0.04	0.04	0.05	0.1
3000	9	0.012	0.08	0.08	0.02	0.0
4000	13	0.012	0.20	0.20	0.02	0.0
—	—	—	—	—	—	—

Table D.2 Random uncertainty bands ($\pm U/2$) for all measured parameters for 10 and 15 km altitudes.

Altitude: 10 km						
Nominal RPM	Measured RPM	Pressure (atm)	Thrust (lb)	Supplied Voltage (V)	Supplied Current (A)	Ambient Temp. (°F)
1000	3	0.010	0.01	0.01	0.02	0.0
2000	6	0.015	0.03	0.03	0.02	0.0
3000	10	0.011	0.09	0.09	0.01	0.0
4000	8	0.016	0.13	0.13	0.02	0.0
5000	28	0.014	0.18	0.18	0.02	0.0
Altitude: 15 km						
Nominal RPM	Measured RPM	Pressure (atm)	Thrust (lb)	Supplied Voltage (V)	Supplied Current (A)	Ambient Temp. (°F)
1000	3	0.004	0.01	0.01	0.02	0.0
2000	6	0.011	0.04	0.04	0.01	0.0
3000	8	0.012	0.08	0.08	0.02	0.0
4000	12	0.003	0.14	0.14	0.02	0.0
5000	22	0.008	0.15	0.15	0.15	0.1

Table D.3 Elemental systematic uncertainty sources and associated bands ($\pm U/2$) for thrust measurements for all altitudes.

Altitude: 0 km				
Nominal RPM	Thrust (lb)			
	Non-Linearity	Repeatability	Hysteresis	Total
1000	0.0125	0.0125	0.01	0.02
2000			0.02	0.02
3000			0.04	0.04
4000			0.07	0.07
5000			0.11	0.11
Altitude: 5 km				
Nominal RPM	Thrust (lb)			
	Non-Linearity	Repeatability	Hysteresis	Total
1000	0.0125	0.0125	0.01	0.02
2000			0.01	0.01
3000			0.03	0.03
4000			0.04	0.04
—			—	—
Altitude: 10 km				
Nominal RPM	Thrust (lb)			
	Non-Linearity	Repeatability	Hysteresis	Total
1000	0.0125	0.0125	0.01	0.02
2000			0.01	0.01
3000			0.02	0.02
4000			0.03	0.03
5000			0.05	0.05
Altitude: 15 km				
Nominal RPM	Thrust (lb)			
	Non-Linearity	Repeatability	Hysteresis	Total
1000	0.0125	0.0125	0.01	0.02
2000			0.01	0.01
3000			0.02	0.02
4000			0.03	0.03
5000			0.05	0.05

Table D.4 Elemental systematic uncertainty sources and associated bands ($\pm U/2$) for electrical and temperature measurements for all altitudes.

Altitude: 0 km			
Nominal RPM	Supplied Voltage (V)	Supplied Current (A)	Ambient Temp. (°F)
	Resolution	Mfc. Spec.	Mfc. Spec.
1000	0.10	0.01	2.3
2000			
3000			
4000			
5000			
Altitude: 5 km			
Nominal RPM	Supplied Voltage (V)	Supplied Current (A)	Ambient Temp. (°F)
	Resolution	Mfc. Spec.	Mfc. Spec.
1000	0.10	0.01	2.3
2000			
3000			
4000			
—			
Altitude: 10 km			
Nominal RPM	Supplied Voltage (V)	Supplied Current (A)	Ambient Temp. (°F)
	Resolution	Mfc. Spec.	Mfc. Spec.
1000	0.10	0.01	2.3
2000			
3000			
4000			
5000			
Altitude: 15 km			
Nominal RPM	Supplied Voltage (V)	Supplied Current (A)	Ambient Temp. (°F)
	Resolution	Mfc. Spec.	Mfc. Spec.
1000	0.10	0.01	2.3
2000			
3000			
4000			
5000			

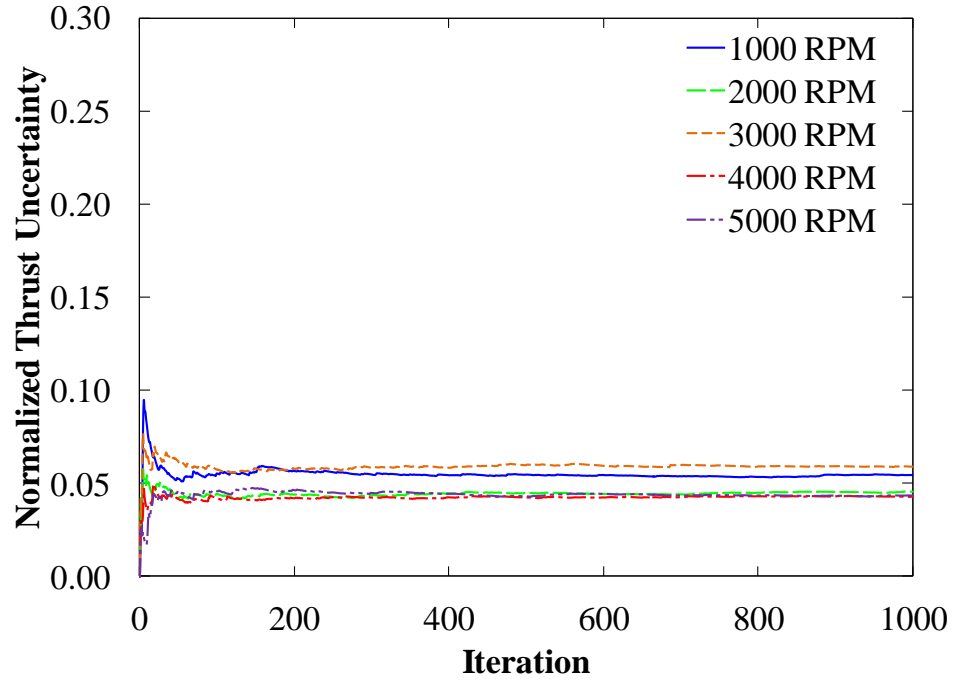


Figure D.1 Convergence of Monte Carlo simulation results for total normalized uncertainty (U_X/X) of thrust for all 0 km tests.

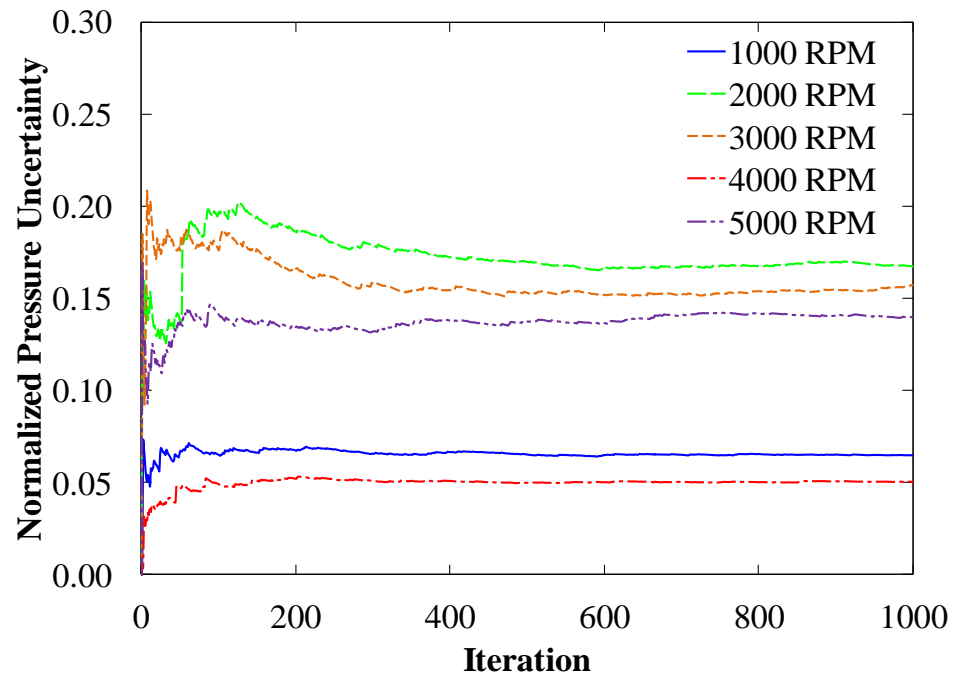


Figure D.2 Convergence of Monte Carlo simulation results for total normalized uncertainty (U_X/X) of pressure for all 15 km tests.

Table D.5 Total uncertainty bands ($\pm U/2$) for all measured parameters for all altitudes.

Altitude: 0 km					
Nominal RPM	Measured RPM	Pressure (atm)	Thrust (lb)	Supplied Power (hp)	Ambient Temp. (°F)
1000	4	0.006	0.02	0.001	2.3
2000	5	0.007	0.08	0.002	2.2
3000	8	0.007	0.22	0.004	2.3
4000	21	0.010	0.3	0.017	2.2
5000	43	0.016	0.5	0.035	2.3
Altitude: 5 km					
Nominal RPM	Measured RPM	Pressure (atm)	Thrust (lb)	Supplied Power (hp)	Ambient Temp. (°F)
1000	5	0.006	0.02	0.001	2.3
2000	6	0.011	0.06	0.001	2.3
3000	9	0.012	0.08	0.003	2.3
4000	13	0.011	0.20	0.006	2.3
—	—	—	—	—	—
Altitude: 10 km					
Nominal RPM	Measured RPM	Pressure (atm)	Thrust (lb)	Supplied Power (hp)	Ambient Temp. (°F)
1000	3	0.009	0.01	0.001	2.2
2000	6	0.015	0.03	0.001	2.2
3000	10	0.010	0.10	0.002	2.4
4000	9	0.016	0.14	0.004	2.2
5000	29	0.013	0.2	0.018	2.4
Altitude: 15 km					
Nominal RPM	Measured RPM	Pressure (atm)	Thrust (lb)	Supplied Power (hp)	Ambient Temp. (°F)
1000	3	0.004	0.01	0.001	2.2
2000	6	0.011	0.04	0.002	2.2
3000	8	0.012	0.08	0.002	2.2
4000	13	0.003	0.14	0.004	2.2
5000	21	0.009	0.16	0.019	2.3

Table D.6 Total uncertainty bands ($\pm U/2$) for all calculated performance parameters for all altitudes.

Altitude: 0 km			
Nominal RPM	Induced Power (hp)	Induced Torque (ft-lb)	Ideal Efficiency
1000	0.000	0.002	0.02
2000	0.003	0.008	0.02
3000	0.014	0.024	0.02
4000	0.024	0.032	0.02
5000	0.051	0.055	0.02
Altitude: 5 km			
Nominal RPM	Induced Power (hp)	Induced Torque (ft-lb)	Ideal Efficiency
1000	0.000	0.002	0.02
2000	0.003	0.007	0.02
3000	0.006	0.011	0.02
4000	0.020	0.026	0.02
—	—	—	—
Altitude: 10 km			
Nominal RPM	Induced Power (hp)	Induced Torque (ft-lb)	Ideal Efficiency
1000	0.000	0.002	0.03
2000	0.003	0.007	0.02
3000	0.009	0.016	0.03
4000	0.023	0.031	0.03
5000	0.038	0.041	0.03
Altitude: 15 km			
Nominal RPM	Induced Power (hp)	Induced Torque (ft-lb)	Ideal Efficiency
1000	0.000	0.003	0.07
2000	0.004	0.012	0.04
3000	0.012	0.021	0.04
4000	0.023	0.030	0.04
5000	0.052	0.055	0.04

Table D.7 Total uncertainty bands ($\pm U/2$) for all calculated dimensionless coefficients for all altitudes.

Altitude: 0 km			
Nominal RPM	Thrust Coeff.	Power Coeff.	Torque Coeff.
1000	0.002	0.001	0.0001
2000	0.002	0.001	0.0001
3000	0.003	0.001	0.0001
4000	0.002	0.001	0.0001
5000	0.003	0.001	0.0002
Altitude: 5 km			
Nominal RPM	Thrust Coeff.	Power Coeff.	Torque Coeff.
1000	0.004	0.002	0.0002
2000	0.004	0.001	0.0002
3000	0.003	0.001	0.0002
4000	0.003	0.001	0.0002
—	—	—	—
Altitude: 10 km			
Nominal RPM	Thrust Coeff.	Power Coeff.	Torque Coeff.
1000	0.007	0.008	0.0005
2000	0.010	0.005	0.0008
3000	0.008	0.003	0.0006
4000	0.011	0.005	0.0009
5000	0.009	0.005	0.0007
Altitude: 15 km			
Nominal RPM	Thrust Coeff.	Power Coeff.	Torque Coeff.
1000	0.014	0.010	0.0014
2000	0.024	0.014	0.0023
3000	0.019	0.009	0.0017
4000	0.011	0.004	0.0011
5000	0.021	0.010	0.0022

Table D.8 Total uncertainty percentages (U_x/X) for all measured parameters for all altitudes.

Altitude: 0 km					
Nominal RPM	Measured RPM	Pressure (atm)	Thrust (lb)	Supplied Power (hp)	Ambient Temp. (°F)
1000	1%	1%	5%	4%	7%
2000	1%	1%	5%	2%	7%
3000	1%	1%	6%	1%	7%
4000	1%	2%	4%	2%	6%
5000	2%	3%	4%	2%	6%
Altitude: 5 km					
Nominal RPM	Measured RPM	Pressure (atm)	Thrust (lb)	Supplied Power (hp)	Ambient Temp. (°F)
1000	1%	2%	8%	4%	7%
2000	1%	4%	5%	1%	7%
3000	1%	5%	4%	1%	7%
4000	1%	4%	5%	1%	6%
—	—	—	—	—	—
Altitude: 10 km					
Nominal RPM	Measured RPM	Pressure (atm)	Thrust (lb)	Supplied Power (hp)	Ambient Temp. (°F)
1000	1%	8%	6%	10%	7%
2000	1%	12%	4%	1%	7%
3000	1%	9%	5%	1%	7%
4000	0%	13%	4%	1%	7%
5000	1%	11%	4%	2%	7%
Altitude: 15 km					
Nominal RPM	Measured RPM	Pressure (atm)	Thrust (lb)	Supplied Power (hp)	Ambient Temp. (°F)
1000	1%	6%	8%	12%	7%
2000	1%	17%	6%	4%	7%
3000	0%	16%	5%	1%	7%
4000	1%	5%	5%	1%	7%
5000	1%	14%	4%	3%	7%

Table D.9 Total uncertainty percentages (U_X/X) for all calculated performance parameters for all altitudes.

Altitude: 0 km			
Nominal RPM	Induced Power (hp)	Induced Torque (ft-lb)	Ideal Efficiency
1000	8%	8%	9%
2000	7%	7%	7%
3000	9%	9%	9%
4000	7%	6%	7%
5000	7%	7%	7%
Altitude: 5 km			
Nominal RPM	Induced Power (hp)	Induced Torque (ft-lb)	Ideal Efficiency
1000	11%	12%	12%
2000	9%	9%	9%
3000	6%	6%	6%
4000	8%	8%	8%
—	—	—	—
Altitude: 10 km			
Nominal RPM	Induced Power (hp)	Induced Torque (ft-lb)	Ideal Efficiency
1000	9%	9%	14%
2000	9%	9%	9%
3000	9%	9%	9%
4000	9%	9%	9%
5000	7%	8%	8%
Altitude: 15 km			
Nominal RPM	Induced Power (hp)	Induced Torque (ft-lb)	Ideal Efficiency
1000	13%	13%	18%
2000	12%	12%	13%
3000	11%	11%	11%
4000	8%	8%	8%
5000	9%	9%	9%

Table D.10 Total uncertainty percentages (U_X/X) for all calculated dimensionless coefficients for all altitudes.

Altitude: 0 km			
Nominal RPM	Thrust Coeff.	Power Coeff.	Torque Coeff.
1000	6%	5%	9%
2000	5%	3%	8%
3000	6%	3%	9%
4000	5%	5%	8%
5000	7%	7%	10%
Altitude: 5 km			
Nominal RPM	Thrust Coeff.	Power Coeff.	Torque Coeff.
1000	8%	6%	13%
2000	7%	5%	11%
3000	6%	5%	9%
4000	7%	5%	10%
—	—	—	—
Altitude: 10 km			
Nominal RPM	Thrust Coeff.	Power Coeff.	Torque Coeff.
1000	10%	13%	15%
2000	13%	12%	19%
3000	10%	9%	14%
4000	14%	14%	21%
5000	12%	12%	18%
Altitude: 15 km			
Nominal RPM	Thrust Coeff.	Power Coeff.	Torque Coeff.
1000	11%	14%	16%
2000	18%	18%	28%
3000	17%	16%	26%
4000	7%	6%	11%
5000	15%	15%	23%

REFERENCES

- [1] Jodeh, N.M., Blue, A.B., and Waldron, A.A., “Development of Small Unmanned Aerial Vehicle Research Platform: Modeling and Simulating with Flight Test Validation,” *AIAA Modeling and Simulation Technologies Conference and Exhibit*, Keystone, Colorado, August 2006, AIAA 2006-6261.
- [2] Corrigan, E.K. and Altman, A., “Survey of Small Unmanned Aerial Vehicle Electric Propulsion Systems,” *46th AIAA Aerospace Sciences Meeting and Exhibit*, Reno, Nevada, January 2008, AIAA 2008-179.
- [3] Logan, M. J., Vranas, T. L., Motter, M., Shams, Q., and Pollock, D. S., “Technology Challenges in Small UAV Development,” AIAA Paper 2005-7089, Sep. 2005.
- [4] Logan, M. J., Chu, J., Motter, M. A., Carter, D. L., Ol, M., and Zeune, C., “Small UAV Research and Evolution in Long Endurance Electric Powered Vehicles,” AIAA Paper 2007-2730, May 2007.
- [5] Ol, M., Zeune, C., and Logan, M., “Analytical-Experimental Comparison for Small Electric Unmanned Air Vehicle Propellers,” AIAA Paper 2008-7345, Aug. 2008.
- [6] Menon, S. K., “Performance Measurement and Scaling in Small Internal Combustion Engines,” M.S. Thesis, Department of Aerospace Engineering, University of Maryland, College Park, 2006.

- [7] Moulton, N. L., "Performance Measurement and Simulation of a Small Internal Combustion Engine," M.S. Thesis, Department of Aerospace Engineering, University of Maryland, College Park, 2007.
- [8] McElroy, T. and Landrum, D.B, "High-Altitude Thermal Testing of a COTS Electric UAV Motor," *2011 Region II AIAA Student Conference*, Tuscaloosa, Alabama, April 2011.
- [9] "F3A Competition Motors," *Hacker Brushless Motors* [commercial web site] URL: <http://www.hacker-motor.com/img/katalog/Hacker2010-2Auflage-web-32-33.pdf> [cited 22 February 2012].
- [10] "MDB-Series Load Cell Specifications," *Transducer Techniques* [commercial web site], URL: <http://www.transducertechniques.com/mdb-load-cell.aspx> [cited 8 December 2011].
- [11] "Instruction Manual for the eLogger V3," *Eagle Tree Systems* [commercial web site], URL: <http://www.eagletreesystems.com/Support/manuals.htm> [cited 11 December 2011].
- [12] "Operating Instructions and Specifications NI DAQ 9211," *National Instruments* [commercial web site], URL: <http://www.ni.com/pdf/manuals/374187c.pdf> [cited 13 December 2011].
- [13] McCormick, B.W., *Aerodynamics, Aeronautics, and Flight Mechanics*, 2nd ed., John Wiley & Sons, New York, 1995, Chap. 6.
- [14] McCormick, B.W., *Aerodynamics of V/STOL Flight*, Academic Press., New York, 1967, Chap. 4.

- [15] Coleman, H.W. and Steele, W.S., *Experimentation, Validation, and Uncertainty Analysis for Engineers*, 3rd ed., John Wiley & Sons, Hoboken, New Jersey, 2009, Chap. 3.